SYNTHESIS OF ^{18}F-RADIOLABELED LLP2A FOR USE IN PET IMAGING VIA ARYLTRIFLUOROBORATE FORMATION

by

Daniel Walker

B.Sc. (Honours), St. Francis Xavier University, 2009

A THESIS SUBMITTED IN PARTIAL FULFILLMENT OF
THE REQUIREMENTS FOR THE DEGREE OF

MASTER OF SCIENCE

in

The Faculty of Graduate Studies

(Chemistry)

THE UNIVERSITY OF BRITISH COLUMBIA

(Vancouver)

July 2012

Abstract

Tumor-specific imaging agents, such as peptides, allow neoplasm visualization by targeting over-expressed extracellular proteins not found on normal cells. This yields not only diagnostic information, but also provide insight into tumor aggressiveness, allowing more accurate treatment and prognosis. LLP2A has been recognized as a strong binder of the $\alpha_4\beta_1$ integrin. Its binding characteristics along with its proteolytic resistance make it an excellent candidate for PET imaging. ^{18}F is widely recognized as the optimal radionuclide for cancer imaging, although its unique chemistry presents difficulties in biomolecule incorporation. The synthesis of ^{18}F-aryltrifluoroborates can be performed under mild conditions, while also creating an imaging agent with triple the specific activity of the source fluoride. Herein is described the synthesis of an ^{18}F-labeled aryltrifluoroborate-LLP2A conjugate, an azide-functionalized LLP2A for use in click radiolabeling, and cellular binding confirmation of the aryltrifluoroborate-LLP2A peptide to $\alpha_4\beta_1$ integrin expressing cells.

Table of Contents

List of Tables

List of Figures

List of Schemes

Abbreviations

α	alpha
β	beta
β^+	positron
δ	delta
λ	lambda
AA	amino acid
ACN	acetonitrile
$ArBF_3$	aryltrifluoroborate
Asc	ascorbate
BOS	beginning of synthesis
BuLi	butyl lithium
D	aspartic acid
DBU	1,8-diazabicycloundec-7-ene
DBF	dibenzofulvene
DCC	N,N'-dicyclohexylcarbodiimide
DCM	dichloromethane
Dde	2-acetyldimedone
DIC	N,N'-diisopropylcarbodiimide
DIPEA	N,N-diisopropylethylamine
DMF	dimethylformamide
DMSO	dimethyl sulfoxide
e^+	positron
e^-	electron
EDC	1-ethyl-3-(3-dimethylaminopropyl)carbodiimide
EDG	electron donating group
EOS	end of synthesis
ESI	electrospray ionization
EtOH	ethanol
eV	electronvolt
EWG	electron withdrawing group
^{18}FDG	^{18}F-2-fluorodeoxyglucose
FITC	fluorescein isothiocyanate
Fmoc	fluorenylmethyloxycarbonyl
Fmoc-Aad(tBu)-OH	Fmoc-2-aminoadipic acid
Fmoc-Ach-OH	1-(Fmoc-amino)cyclohexanecarboxylic acid
G	glycine
HATU	O-(7-azaBenzotriazole-1-yl)-1,1,3,3-tetramethyluronium hexafluorophosphate
HBTU	O-(Benzotriazole-1-yl)-1,1,3,3-tetramethyluronium hexafluorophosphate

HCTU	O-(6-chlorobenzotriazole-1-yl)-1,1,3,3-tetramethyluronium hexafluorophosphate
HFIP	hexafluoro-2-propanol
HOBt	hydroxybenzotriazole
HRMS	high resolution mass spectrometry
IC_{50}	half maximal inhibitory concentration
J	coupling constant
L	leucine
LRMS	low resolution mass spectrometry
Lys	lysine
m/z	mass-to-charge ratio
MMP	matrix metalloproteinase
MRI	magnetic resonance imaging
MS	mass spectrometry
NHS	N-Hydroxysuccinimide
NIR	near infrared
NIRF	near infrared fluorescence
NMR	nuclear magnetic resonance
Nu	nucleophile
o	ortho
PET	positron emission tomography
PG	protecting group
ppm	parts per million
R	arginine
R_f	retardation factor
RBF	round-bottomed flask
RP-HPLC	reverse-phase high performance liquid chromatography
RT	room temperature
SA	specific activity
SPECT	single photon emission tomography
SPPS	solid phase peptide synthesis
$t_{1/2}$	half-life
t_R	retention time
TBS	tris buffered saline
*t*Bu	*tert*-butyl
TFA	trifluoroacetic acid
THF	tetrahydrofuran
TLC	thin layer chromatography
UV	ultraviolet
V	valine

Acknowledgements

First and foremost, I would like to express my gratitude to my supervisor, Dr. David M. Perrin. His passion for science and work ethic are qualities I will continue to admire for years to come. I would like to thank Dr. Perrin for his encouragement, scientific insight, and helpful teachings over the course of this project.

I would like to thank Dr. Ying Li, formerly of the Perrin group, for all of her leadership and assistance with this project. I would like to thank all my fellow group members for making my research an enjoyable experience and allowing my education at UBC to include more than only scientific studies.

Most of all, I would like to thank my family for providing me with the love, kindness, support, and foundation necessary to pursue my education.

Chapter 1

Introduction

1.1 Cancer and its Imaging

1.1.1 A Brief Overview of Cancer

Cancer can be defined as a group of cells that exhibit uncontrolled division. These cells often metastasize, invading neighboring tissue and spreading to other parts of the body via the lymphatic system and the bloodstream. The malignancy may grow and destroys healthy tissue until necessary organs are unable to function, which proves fatal to the patient. Cancer is among the leading causes of death in the developed world and the second leading cause of death in developing countries.[1] In Canada, 29 % of deaths annually are related to cancer. The incidence and mortality rates for cancer in Canada have both recently been on the rise, increasing by 1.6 and 1.2 %, respectively, from 2009 to 2010.[2] A disease with the global reach of that of cancer is rare and its increasing prevalence is cause for concern. In light of this, research investigating all aspects of this broad disease has also been growing. Increased insight into cancer's epidemiology, diagnosis, and treatment will hopefully give rise to a diminished incidence of cancer and advancements in patient care in the near future.

There are many ways that cancer can be diagnosed, usually beginning with the patient noticing signs and symptoms. If cancer is suspected, several tests are done before making further conclusions, including imaging and blood screens. The diagnosis

may then be confirmed by a histological examination of the neoplastic tissue performed by a pathologist. Cancer can be treated by a variety of methods ranging from surgery to radiation therapy to chemotherapy, among others. To many people, the word cancer is synonymous with death, although mortality rates differ widely among various types of cancer.[2]

1.1.2 Cancer Imaging Technology

An aging population coupled with an increasing incidence of cancer means that novel and effective methods of diagnosing and treating cancer are more essential now than ever. One way to monitor the progression of cancer is via techniques that can create a visual image of the neoplasm itself. The most common imaging techniques used today are magnetic resonance imaging (MRI), single photon emission computed tomography (SPECT) and positron emission tomography (PET).

MRI is used to image bodily structures without the use of ionizing radiation, which minimizes the risk to the patient. Rather, it employs the nuclear magnetic resonance properties of the atoms that make up the tissue and also uses a contrast agent to improve internal visibility. These contrast agents are most often gadolinium based. Unfortunately, the sensitivity to these contrast agents is low and this has prevented MRI from being considered among the best techniques for molecular imaging of localized and microscopic disease.[3] This technique is also not suited for patients with pacemakers or certain metallic implants due to the strong magnetic field that is employed.

SPECT produces images via the emission of a single gamma ray that is measured directly by the detector. The emission energy of these gamma rays is too high to be absorbed by body tissues, ergo decreasing the radiation absorption by the patient. Long half-life isotopes may be used for SPECT, enabling more synthetic freedom and time for distribution of labeled compounds. This also extends timeframes for imaging, permitting physicians to observe *in vivo* processes within hours of or even days after injection.[4, 5] The need for a second dose of radiotracer is also eliminated, should follow-up scans be required shortly after the initial imaging. The main limitation of SPECT is its sensitivity; i.e. the percentage of emitted photons that are actually detected and used to construct an image. This arises because a collimator is required to absorb photons that are outside of the angular range of the detector, causing only a small number of photons to reach the detector. Due to this necessity, the efficiency of SPECT is approximately 0.01 %.[5]

PET is able to produce high resolution, three-dimensional images of cancerous tissue using nuclides that emit positrons. When a positron is emitted, it travels a short distance (the positron range) until it loses enough energy that it can interact with an electron. At this point, a collision occurs, resulting in annihilation and producing two gamma photons of 511 keV each. These two photons are emitted at 180° to each other and are detected coincidently, increasing the acceptable detection angle and eliminating the need for a collimators. This results in a sensitivity of about 1 %.[5, 6] The resolution of the image depends on the distance travelled by the positron prior to annihilation, which is directly proportional to positron energy. By labeling a cancer targeting biomolecule

with a positron-emitting isotope, this decay can be localized and an image generated. Although PET is able to produce some of the highest quality molecular images, it is handicapped by the high production cost of imaging agents and the scanners themselves.[7, 8]

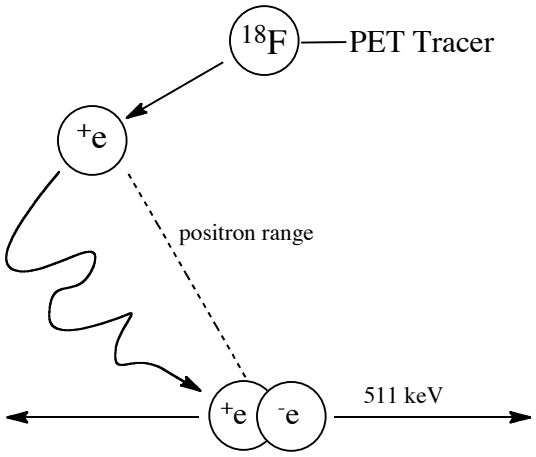

Figure 1.1: Positron ($^{+}$e) emission by ^{18}F followed by collision with an electron ($^{-}$e), resulting in annihilation of both particles and producing two gamma rays of 511 keV each.

1.1.3 PET Isotopes

The choice of isotope for PET imaging depends on several properties:[9] 1) a low positron energy that will yield a short positron range and therefore good image resolution, 2) a moderate half-life that allows enough time for incorporation into a biomolecule without significant loss of specific activity but not so long that the patient experiences harmful radiation absorption post-imaging, 3) a clean decay process consisting of mostly positron decay, and 4) the ease of production of the radioisotope and its intrinsic chemical properties allowing for simple and reproducible methods of incorporation.

There are several isotopes that are potentially suitable for use in PET imaging; selected isotopes are outlined in Table 1.1. ^{11}C would be an excellent isotope for PET imaging due to its high specific activity and percentage of β^+ decay, however its half-life is often too short for synthesis and distribution.[9] ^{64}Cu and ^{68}Ga are of interest because these can be easily incorporated into biomolecules through the use of chelators. Simply mixing the imaging compound in a solution of the metal is enough to almost fully incorporate it. However, ^{64}Cu does not exhibit a clean decay process which results in a low percentage of β^+ decay and thus requires longer acquisition times[10]. ^{68}Ga has a high positron emission energy, consequently decreasing the resolution of the resulting images. All things considered, it becomes apparent that ^{18}F is the ideal isotope to be used in PET imaging due to its low positron energy, clean decay process and moderate half-life.[9, 11] In light of these properties, ^{18}F has become the most commonly used isotope for PET imaging, employed in the form of ^{18}F-2-fluorodeoxyglucose (^{18}FDG).

Table 1.1: Properties of several possible isotopes for use in PET imaging.[9]

Nuclide	$t_{1/2}$ (min)	SA (Ci/μmol)	Decay (% β^+)	β^+ energy (MeV)		β^+ range in Water (mm)	
				Max.	Mean	Max.	Mean
^{64}Cu	768	245	17.9	0.65	0.28	2.9	0.64
^{68}Ga	68	2766	87.7	1.90	0.84	8.2	2.9
^{11}C	20	9220	99.8	0.96	0.39	4.1	1.1
^{18}F	110	1710	96.7	0.63	0.25	2.4	0.6

1.1.4 ^{18}F Production

^{18}F can be produced in different ways, depending on whether it is to be incorporated into the biomolecule as an electrophile or as a nucleophile. For electrophilic incorporation, $^{18}O_2$ gas is converted to $^{18}F_2$ by proton bombardment.[11] Elemental fluorine is highly reactive, providing a rapid labeling reaction that limits radioactive decay and loss of specific activity. This reactivity, as well as its gaseous state makes $^{18}F_2$ difficult to prepare and handle, resulting in electrophilic incorporation being rarely used. In addition, electrophilic fluorine is produced at low specific activity. The preferred method is nucleophilic incorporation. Here, $H_2{}^{18}O$ is bombarded with a proton beam to produce $^{18}F^-$. The ^{18}F anion is then separated out using an anion exchange column and usually stabilized by adding a crown ether, 2,2,2-cryptand, and eluted.[11] This ^{18}F anion can then be used to radiolabel biomolecules by nucleophilic displacement reactions.

1.1.5 ^{18}FDG

^{18}FDG is an analog of 2-deoxyglucose on which an ^{18}F atom is installed at the 2' position instead of the normal hydroxyl group present in glucose. ^{18}FDG is injected into the bloodstream of a patient and is then imported into cells via specific transporters on the cell membrane. It then undergoes phosphorylation within the cytosol at the C-6 position by the enzyme hexokinase.[12] There are two reasons why this is useful for imaging purposes. First, cancer cells are rapidly growing and exhibit accelerated glucose metabolism compared to normal cells, causing ^{18}FDG to become more concentrated in

cancerous tissue. Second, due to the absent 2' hydroxyl group, the ^{18}FDG cannot be metabolized further. Following phosphorylation at the C-6 position, the molecule is charged and must remain in the cell.[7, 13] With the ^{18}FDG localized and trapped within the cancer cells, an image may be produced in which malignant tissue is identified by locating the areas of concentrated radioactive decay.

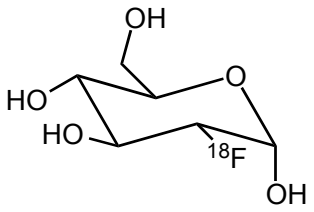

Figure 1.2: The structure of ^{18}FDG. The 2'-OH of glucose is replaced with ^{18}F to allow for PET imaging.

1.1.6 Tumor-Specific Imaging

While the use of ^{18}FDG to image cancer is an extraordinary breakthrough in diagnostic nuclear medicine, it has several drawbacks. It is often difficult to visualize malignant tissue contained within areas of the body that have a naturally high glucose uptake, such as the brain, myocardium, muscles, and urinary tract.[7, 12] Therefore, ^{18}FDG is only useful for imaging once the tumor has reached a minimum size to allow sufficient ^{18}FDG accumulation, permitting suitable differentiation against the background. Perhaps the biggest drawback of ^{18}FDG is that it is rather non-specific; it does not help elucidate any information about patient-specific tumor biology.[9]

By using radiopharmaceuticals that are specific to different types of cancer, more specific phenotypes may be characterized.[14] This allows PET imaging to not only be useful for imaging the tumor, but for choosing the appropriate treatment option by

offering information about tumor aggressiveness and proliferation. By diagnosing cancerous tissue earlier and more specifically, the survival rate of the patient is increased and the overall cost of care is decreased.[2] In order to provide this specific imaging, radiolabeled biomolecules such as peptides or oligonucleotides that exhibit a high affinity for extracellular markers present in the early stages of specific cancers could be used.

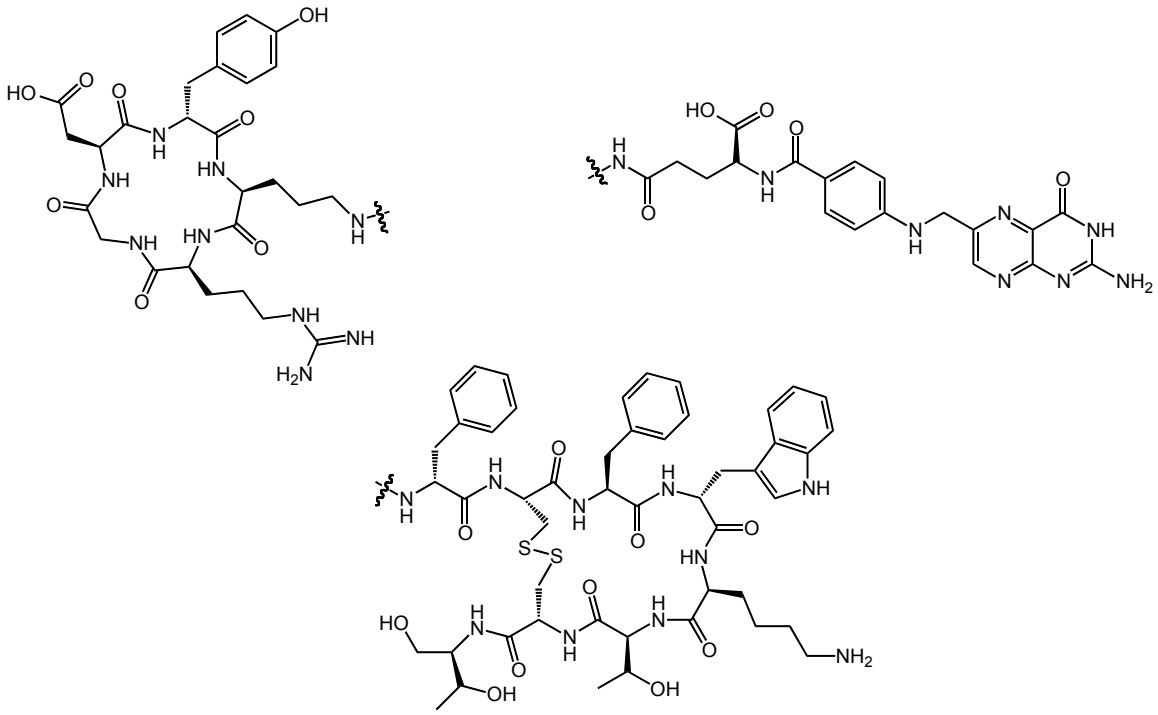

Figure 1.3: Select peptides currently under investigation for molecular imaging purposes. RGD[15] (top left), folic acid[16] (top right), and octreotide[17] (bottom) are shown. A radioactive imaging moiety would be attached at the interrupted bond to enable PET imaging.

A covalent bond between the ^{18}F atom and the tumor-targeting biomolecule is necessary for PET imaging since the radioisotope must remain anchored to the imaging agent at all times in order to produce a clear, high resolution image. Cleavage of the

^{18}F-biomolecule bond will result in the free radionuclide itself being tracked by the imaging device, as opposed to nuclide-biomolecule conjugate. In the absence of the biomolecule, the radionuclide has no ability to localize at the malignancy, thus defeating the purpose of the imaging scan. To form a covalent ^{18}F-C bond, as found in ^{18}FDG, harsh reaction conditions including high temperatures and aprotic, organic solvents are usually required in order to increase the nucleophilicity of the ^{18}F anion.[11, 18] These conditions are generally not compatible with biomolecules, which normally must be stored under mild physiological conditions, and therefore could possibly lead to an alteration of their biological activity and loss of imaging functionality.

Despite these concerns, studies on direct ^{18}F-labeling of biomolecules have appeared in the literature.[19-21] Chen *et al.* have recently reported a one-step ^{18}F-labeling strategy that involves ^{18}F-C bond formation via aromatic nucleophilic displacement.[21] Activation of a nitro group by an *ortho* trifluoromethyl substituent provides sufficient electron withdrawing properties to allow nucleophilic substitution of NO_2 by fluoride at high temperature.

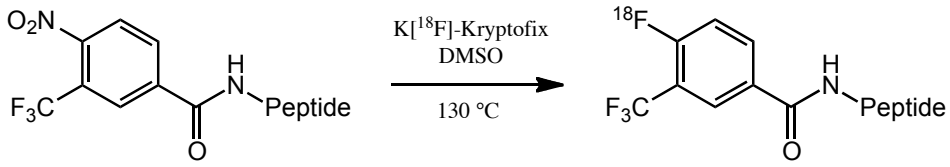

Scheme 1.1: One-step ^{18}F-labeling strategy proposed by Chen *et al.*

This method was tested by incorporating the nitro-arene moiety into the cyclic RGD peptide (shown in Figure 1.3), a well-known ligand for the $\alpha_5\beta_3$ integrin. Predictably, Chen *et al.* observe that the high temperature (130 °C) of the labeling reaction resulted in decomposition of the peptide, as is evident in the RP-HPLC traces (Figure 1.4). Not only are there several ^{18}F-labeled products, unlabeled peaks are also observed by UV detection which indicates the breakdown of the peptide at a number of positions. Significant difficulty in separating the ^{18}F-labeled products from the nitro precursors is also mentioned. This method is an interesting study of a one-step ^{18}F-labeling for use in PET imaging, but the aforementioned drawbacks demonstrate the necessity of an alternate route for viable ^{18}F-labeling of biomolecules.

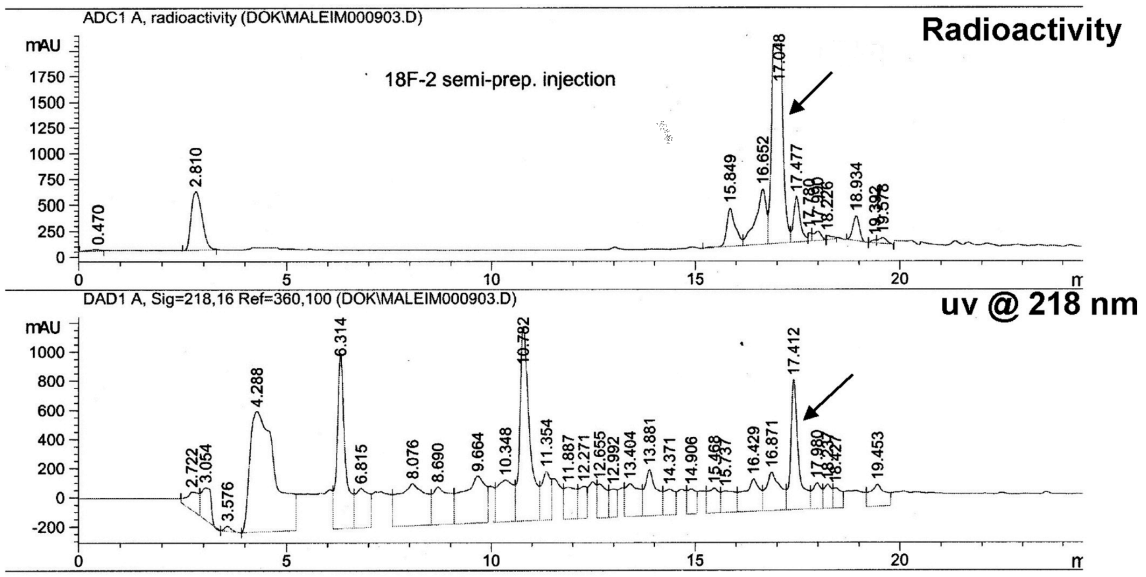

Figure 1.4: RP-HPLC traces of the one-step ^{18}F-labeling of RGD via nucleophilic aromatic substitution by Chen *et al*.[21] The arrow indicates the desired product. Reproduced from Chen *et al*. w/o permission.

1.1.7 Alternative ^{18}F-Labeling Strategies

Current ^{18}F-labeling strategies are focused on first labeling a synthon, in which an activated group is exchanged for ^{18}F via nucleophilic displacement, then undergoing further reaction to conjugate the snython to the bioactive moiety. This allows the biomolecule to bypass the harsh conditions required to complete a nucleophilic substitution reaction using ^{18}F. An example of this strategy for labeling antibodies performed by Zalutsky[22] is shown in Scheme 1.2 below.

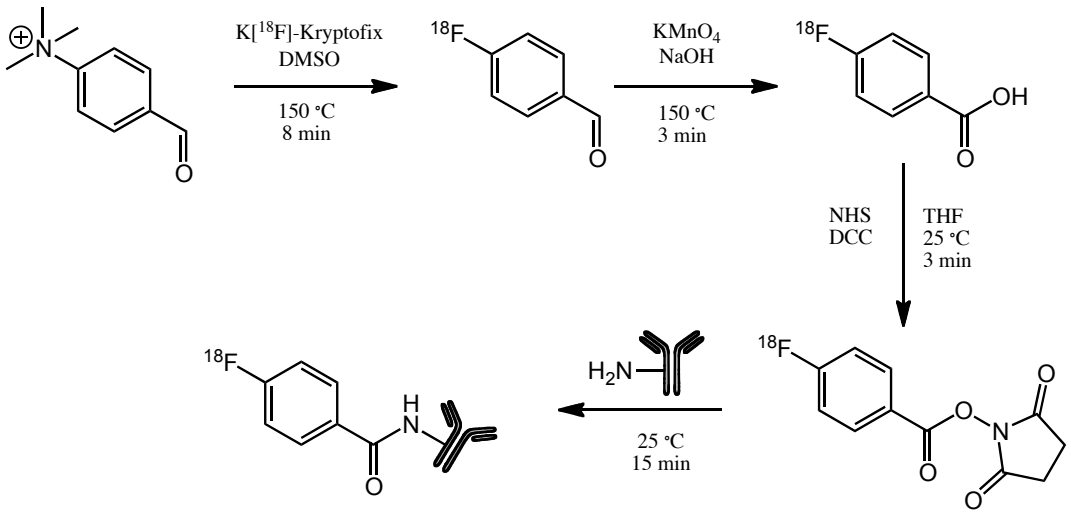

Scheme 1.2: A multi-step ^{18}F-labeling scheme employing $^{18}F^-$ in a nucleophilic substitution reaction, followed by NHS ester formation and subsequent antibody coupling.

The main drawback with this method is the number of steps, and ensuing purifications that are required. The purity of any radio-imaging agent is of the utmost importance, meaning purification must achieve >95 % purity. Multi-step reaction schemes and lengthy purification to prepare a sample for PET imaging causes a decrease

in specific activity due to the radioactive decay occurring simultaneously. This, in turn, yields a diminished image quality and necessitates a higher dosage of the drug. For these reasons, click chemistry has recently become of interest to the PET labeling community[23-26] due to its robust nature, mild conditions and complete conversion.[27] The Huisgen cycloaddition, the premier click reaction, provides a facile method for connecting a radiolabeled synthon with a biomolecule through the formation of a 1,2,3-triazole by 1,3-dipolar cycloaddition between an alkyne and an azide. A typical click radiolabeling strategy is shown below.

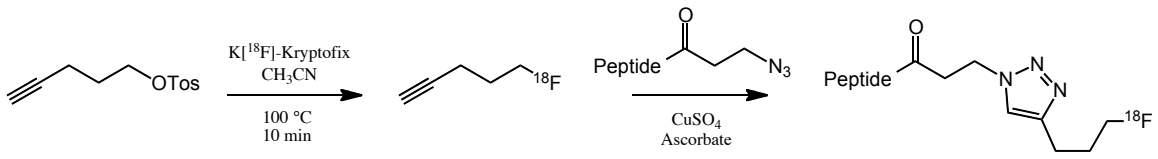

Scheme 1.3: Two-step biomolecule radiolabeling via click conjugation.

Although the click strategy increases simplicity by minimizing the number of steps and purification, there remains room for improvement. The ideal biomolecule labeling reaction would be a one-step reaction that takes place under mild conditions and affords simple purification with minimal byproducts. A method able to fulfill these criteria could push the boundaries of PET image technology further than previously thought possible.

1.2 Arylborates as Fluoride Captors

1.2.1 Advantages of Trifluoroborates

It has been shown that trifluoroborates can be synthesized from boronic acids under mild aqueous conditions.[28] In accord with these findings, Perrin and colleagues have hypothesized that fluoride capture by boron may be applicable to radiopharmaceuticals.[29] Perrin *et al.* were able to show ^{18}F incorporation into an aryl moiety through the formation of an ^{18}F-aryltrifluoroborate. The advantages to this strategy are threefold. By labeling a biomolecule in one step, the number of side products may be greatly reduced, decreasing purification times and thereby increasing yield. Furthermore, a rapid, one-step reaction favors the medium length half life of ^{18}F, allowing bioconjugates of good specific activity to be produced. Lastly, three fluoride atoms are incorporated in a trifluoroborate, in contrast to one fluoride seen in current labeling strategies. By incorporating three fluoride atoms onto a single molecule the specific activity is tripled, allowing the synthesis of compounds attaining previously impossible specific activities and yielding greatly enhanced images.

Another attraction of fluoride capture via boron, which plays to the economics of PET imaging, is the fact that these boronate-biomolecule conjugates could be premade and stored on-site prior to labeling. One could envision the delivery of aqueous ^{18}F which could then be reacted with the bioconjugate using a simple aqueous wash-in immediately prior to injection into the patient. The ability to produce boron bioconjugates for imaging different types of cancer in a “kit-like” fashion could lead to decreased operating costs for hospitals and radiopharmaceutical companies alike. This,

in turn, will make PET imaging technology more widely available to those who might otherwise not have access to this era's optimum cancer imaging technique.

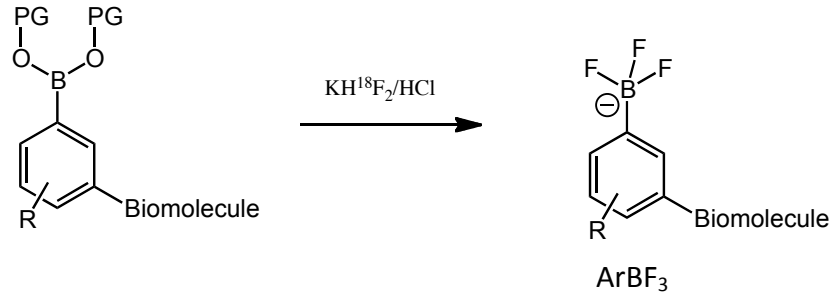

Scheme 1.4: General scheme of fluoride capture by a protected arylborate to produce an aryltrifluoroborate ($ArBF_3$).

1.2.2 Stability of Aryltrifluoroborates

As mentioned previously, it is important that the ^{18}F atom does not dissociate from the biomolecule on the imaging timescale. For this reason, the stability of several aryltrifluoroborates was studied by Dr. Richard Ting, previously of the Perrin group.[30, 31] It is proposed that decomposition of aryltrifluoroborates under aqueous conditions would first see the elimination of one fluoride atom, bringing the boron to a neutral charge with sp^2 hybridization. This is followed by nucleophilic attack of a water molecule at the vacant p orbital. Another water molecule is added and the process is repeated, concluding in the formation of a boronic acid and complete solvolytic liberation of the remaining fluorides.

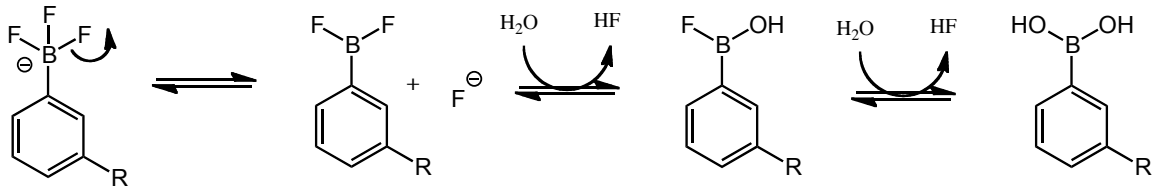

Scheme 1.5: Mechanism of hydrolysis of an aryltrifluoroborate. R group represents bioactive moiety such as a peptide or antibody.

The effect of electron withdrawing groups on aryltrifluoroborate hydrolysis was investigated by the Perrin group using a Hammet analysis.[31] The results of the experiments suggested that electron withdrawing groups (EWGs) in the *para* and *meta* position to the trifluoroborate group slowed the defluorination while electron donating groups (EDGs) in the *para* position enhanced the rate of solvolysis of aryltrifluoroborates. Rationalization of this can be achieved through observing charge localization of the resonance structures of aryl rings substituted with electron withdrawing and electron donating groups. EWGs are able to stabilize the negatively charged boron of the trifluoroborate by localizing a partial positive charge on the adjacent carbon, resulting in slower B-F solvolysis.

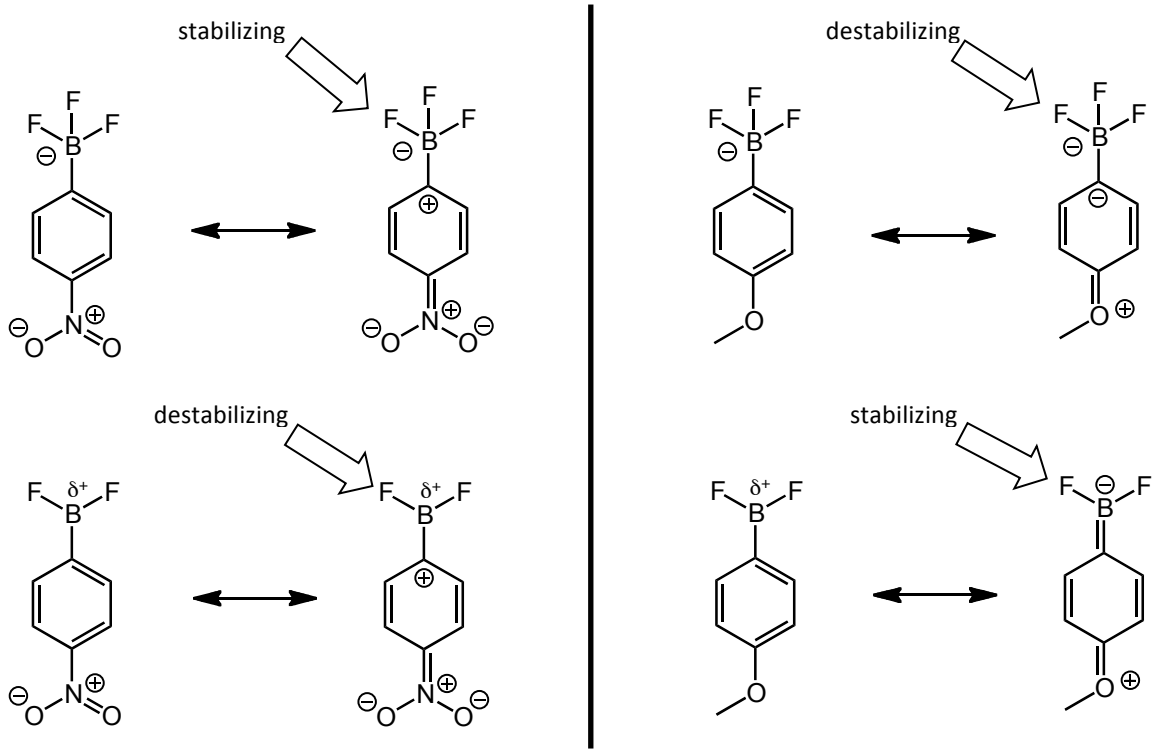

Figure 1.5: Charge distribution of electron donating and withdrawing substituents on aryltrifluoroborates leading to increased or decreased rate of fluoride dissociation.

EDGs have the opposite effect. Accumulation of electron density on the carbon adjacent to the negatively charged trifluoroborate destabilizes the trifluoroborate and enhances the rate of fluoride dissociation. Loss of fluoride from the aryltrifluoroborate yields an aryldifluoroborate in which the boron is sp^2 hybridized with an empty p orbital (see Scheme 1.5). This aryldifluoroborate is further stabilized by EDGs, which can distribute electron density into the empty p orbital. EWGs would again have the opposite effect, destabilizing the aryldifluoroborate by localizing positive charge next to the vacant p orbital of boron. Altogether, EWGs stabilize the aryltrifluoroborates and destabilize the transition state for solvolysis that would be similar to the aryldifluoroborate ground state. This leads to slower aryltrifluoroborate solvolysis and,

importantly, a more stable imaging agent. Out of several commercially available aryl boronic acids, it was found that *ortho* and *para* fluorine-substituted aryltrifluoroborate exhibited a significantly decreased rate of aryltrifluoroborate solvolysis.

A conjugatable handle is also required to link the aryltrifluoroborate to the biomolecule. In this case, a carboxylic acid would be useful due to its facile coupling through amide bond formation, as well as its electron withdrawing properties which provide further stabilization of the B-F bond. By placing each of these electron withdrawing groups on the aryl ring it was hypothesized that this species would be capable of stabilizing the negative charge of a trifluoroborate.

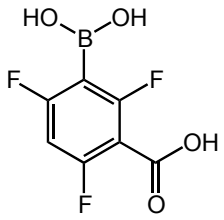

Figure 1.6: Structure of the boronic acid to be used for fluoride labeling studies.

1.2.3 Boronic Acid Protecting Groups

In order to prevent unwanted chemistry from occurring at the boronic acid site during the coupling of the imaging moiety to the biomolecule, a protecting group is also needed. The protecting group needs to be acid-labile such that removal occurs simultaneously with the radiolabeling, while also preferably protecting both hydroxyl groups on the boron. Taking into account these conditions, the Perrin group

investigated pinacol and 1,1,2,2-tetraphenyl pinacol as possible protecting groups. The C-B bond was found to be unstable in basic conditions when pinacol was employed as a protecting group. It was hypothesized that base-mediated deboronation occurred when the boron adopted a tetrahedral geometry. In order to counteract this, 1,1,2,2-tetraphenyl pinacol was used to add steric bulk, inhibiting the formation of the tetrahedral borate anion and increasing the stability of this species. With these findings in mind, a synthetic avenue towards 2,4,6-trifluoro-3-(4,4,5,5-tetraphenyl-1,3,2-dioxaborolan-2-yl)benzoic acid (henceforth referred to as $ArB(OR)_2$) was devised.[32]

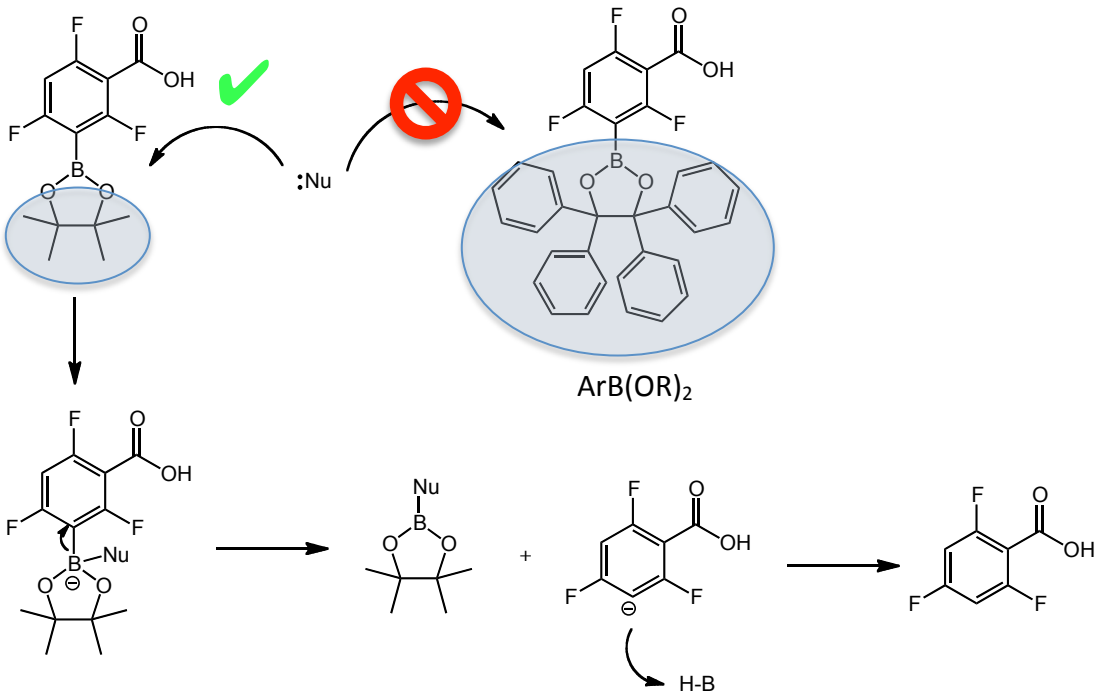

Figure 1.7: Prevention of C-B bond cleavage by base-mediated deboronation through use of a sterically encumbered protecting group.

1.2.4 $ArB^{18}F_3$-marimistat

After confirming that the $ArB^{18}F_3$s were stable *in vivo,*[32] the first neoplastic tissue PET imaging test of arylborates as fluoride captors was done through conjugation to marimastat, a clinically trialed broad spectrum matrix metalloproteinase (MMP) inhibitor.[33] The arylborate was conjugated through amide formation via a small linker attached to the marimastat.[34] This compound was converted to the radiolabeled aryltrifluoroborate and imaged *in vivo* in mice that had been xenografted with murine breast carcinomas (Figure 1.8). While the overall results of this imaging were positive, there was room for improvement. Although localization around the malignant tissue was observed, the quality of the image was lacking. The increase in contrast required to make the image viable was inconsistent with the current standard for PET imaging. It was concluded that the low image quality was a product of the broad spectrum nature of marimistat itself. High uptake of the drug was observed in tissues with known non-pathologic MMP expression such as the liver as well as the blood, yielding a poor target/non-target contrast.[34] While the results of the $ArB^{18}F_3$-marimistat imaging were encouraging with respect to the aryltrifluoroborate strategy, a new bioactive moiety was required for further imaging investigation.

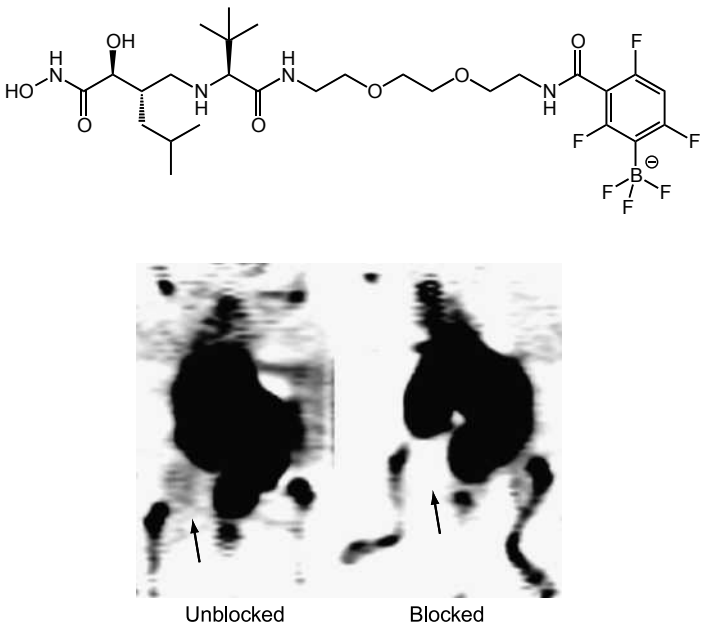

Figure 1.8: Structure of $ArB^{18}F_3$-marimistat (top) and *in vivo* imaging results (bottom) of murine breast carcinoma.

1.3 LLP2A

1.3.1 The $\alpha_4\beta_1$ Integrin

Cellular surface proteins are good targets for candidate imaging agents due to their over-expression by many types of malignancies.[35] The $\alpha_4\beta_1$ integrin has been identified as a regulator of tumor growth, metastasis and angiogenesis.[36] Antibodies against this integrin have been effective in inhibiting tumor growth due to its over-expression during these phases.[37] The $\alpha_4\beta_1$ integrin has been found in leukemias, lymphomas, melanomas and sarcomas, making it an ideal target for cancer imaging studies.

1.3.2 High-Affinity $\alpha_4\beta_1$ Ligand Identification

The Kit Lam lab at UC Davis discovered a high-affinity and high-specificity ligand for imaging the $\alpha_4\beta_1$ integrin.[38] This was done through a one-bead-one-compound combinatorial library,[39, 40] in which each bead contains one discrete peptide. This library was designed around the LDV motif[41] and the 2-(4-(3-*o*-toylureido)phenyl)acetic acid N-terminal cap,[42] which greatly enhances LDV interaction and decreases proteolysis. Through diversification at each position, X_1-X_5, the binding abilities of many individual peptides were screened. The urea terminal cap was diversified using 420 combinations of 30 isocyanates and 14 4-amino phenyl acetic acids at the X_1 and X_2 positions, respectively. The LDV motif was diversified using 6 leucine and 20 lysine analogs at X_3, 3 aspartic acid analogs at X_4, and 18 valine analogs at X_5.

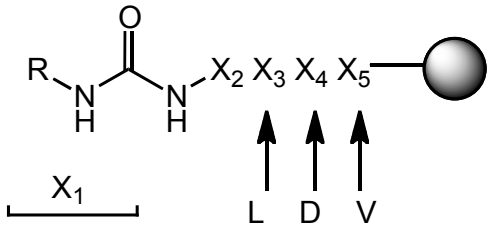

Figure 1.9: The structure of the library design for the screening of $\alpha_4\beta_1$ targeting ligands.[38]

To test the affinity of the randomized discrete peptides, the beads were exposed to $\alpha_4\beta_1$ expressing Jurkat cells. The beads which localized around cells exhibited superior binding characteristics and their peptide sequences were elucidated. In order to further select for the highest affinity ligands, an increasing amount of a known $\alpha_4\beta_1$

antagonist[42] was added into the screening solution. This competition assay between the antagonist and the synthetic ligand was able to isolate one high-affinity peptide sequence, henceforth denoted as LLP2A (Figure 1.10). LLP2A was determined to have an IC_{50} of 2.0 ± 1.4 pM.[38] A low IC_{50} value improves imaging by better localizing the drug and limiting the amount of background radiation seen, while also decreasing the amount of imaging agent required to obtain a viable, high quality image.

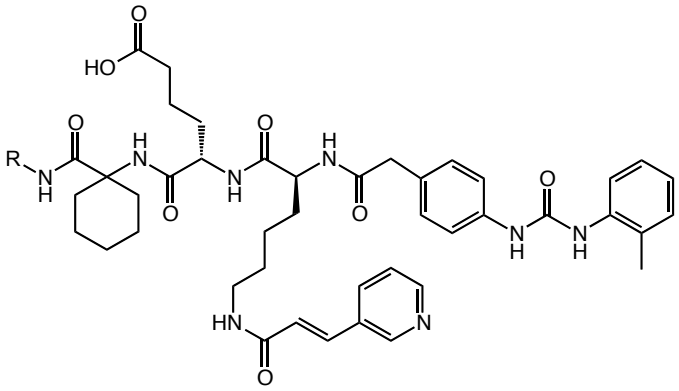

Figure 1.10: The structure of LLP2A, a high-affinity ligand for the $\alpha_4\beta_1$ integrin. R represents an imaging moiety for PET, SPECT, fluorescence or other.

1.3.3 *In Vivo* Testing of LLP2A

To continue investigation of this compound and demonstrate its targeting abilities, the Lam group conjugated LLP2A to Cy5.5,[43] a fluorophore emitting in the near infrared (NIR) region. Molt-4 leukemia cells expressing the $\alpha_4\beta_1$ integrin were xenografted into mice and the Cy5.5-LLP2A conjugate was injected when the tumor had reached approximately 0.8 cm in diameter. The tumor was then analyzed both *in vivo* and *ex vivo* by NIR fluorescence (NIRF); the results of both showed fluorescence was observed

in the malignant tissue with low uptake in other organs (Figure 1.11).[43] These positive findings, along with its low IC_{50} and proteolytic resistance due to its unnatural amino acid composition, cemented LLP2A as an excellent candidate for further research into the applicability of arylborates as fluoride captors for PET imaging.

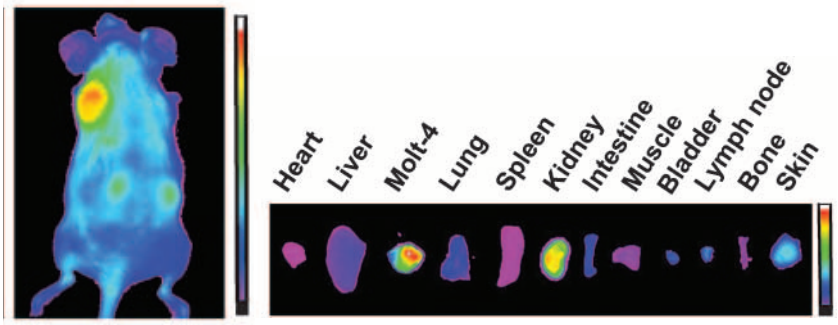

Figure 1.11: Localization of Cy5.5-LLP2A in $\alpha_4\beta_1$ expressing Molt-4 cells.[43] a) *in vivo* NIRF image, b) NIRF image of excised tumor and organs. Reproduced from Lam *et al.* w/o permission.

1.4 ArB(OR)$_2$-LLP2A Synthetic Strategy

1.4.1 One-step Strategy

In light of the advantageous properties of LLP2A, a synthetic strategy to conjugate this peptide with an arylborate was designed. If both LLP2A and the arylborate possess carboxylic acid functional groups, these two could be joined through amide formation with a bis-amino terminally functionalized linker. The final project target, ArB(OR)$_2$-LLP2A, and retrosynthetic analysis is shown in Figure 1.12.

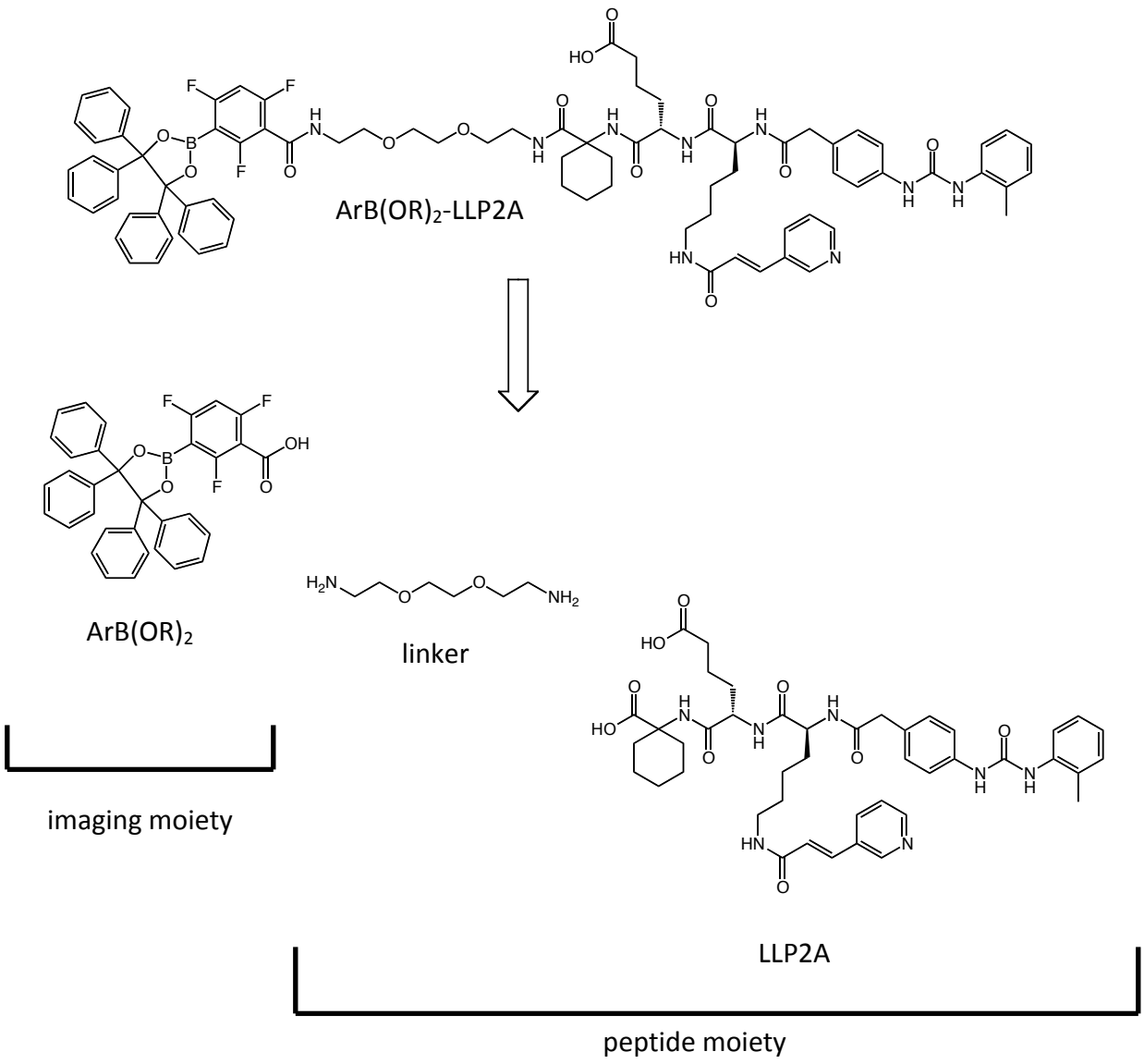

Figure 1.12: Structure of the target molecule, $ArB(OR)_2$-LLP2A, and its retrosynthetic analysis.

The peptide moiety could be synthesized by standard solid phase peptide synthesis using Fmoc protecting group chemistry. The solid phase resin was purchased preloaded with the desired linker, allowing synthesis of the peptide at one end and

subsequent cleavage from the resin to produce the terminal amine. After the completion of the peptide moiety, the arylborate would be conjugated to the peptide via an amide forming coupling reaction. The finished molecule could then be fluorinated and its biological activity confirmed through a cellular binding assay. To do this, a fluorescent version of the peptide would need to be created. Incubating $\alpha_4\beta_1$ expressing cells with a fluorescent LLP2A would allow for visual binding confirmation using fluorescence microscopy. A positive result from this experiment would pave the way for radiolabeling and *in vivo* imaging studies.

1.4.2 Two-step Strategy

A clickable version of LLP2A is also envisaged to allow for studies of a two-step one-pot labeling reaction through 1,2,3-triazole formation. The same peptide moiety could be functionalized with an azide by coupling a small, straight-chained azido-carboxylic acid. This would permit the radiolabeling of an alkynyl arylborate, followed by click conjugation to the peptide moiety in the same reaction vessel. The final labeled product and retrosynthesis is found in Figure 1.13.

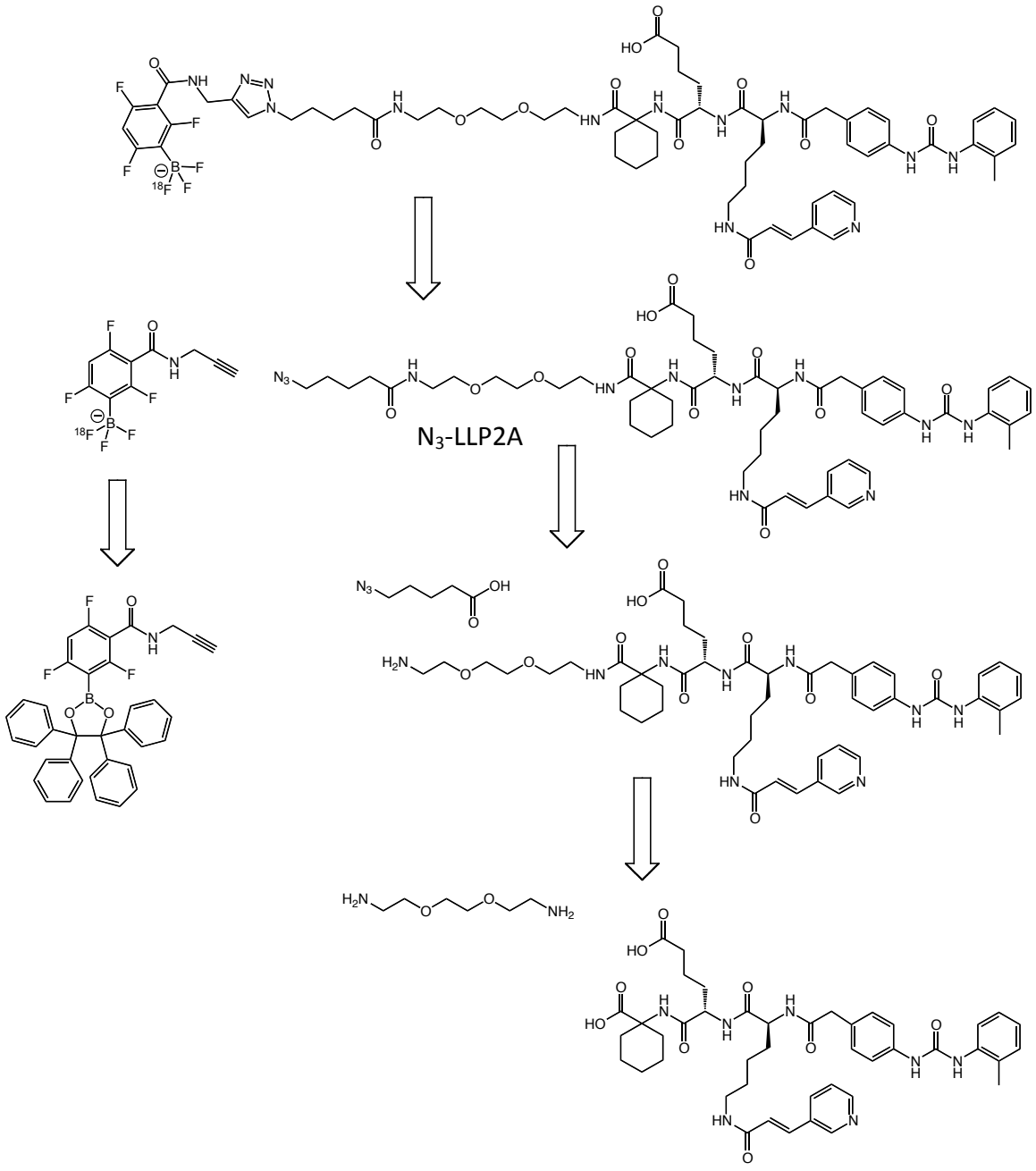

Figure 1.13: Retrosynthetic analysis of ^{18}F-labeling of N_3-LLP2A via click chemistry.

Chapter 2

Results and Discussion

2.1 Peptide Synthetic Strategy

2.1.1 Solid Phase Peptide Synthesis (SPPS) Overview

The synthesis of LLP2A was done on the solid phase using the Fmoc protecting group strategy,[44] summarized below in Scheme 2.1. Briefly, the first amino acid (AA1) in the sequence is installed on the resin via amide formation utilizing a coupling agent, then the Fmoc protecting group is removed by washing with a 20 % piperidine in DMF solution. This affords a free terminal amine, at which point the next amino acid (AA2) can be added using the same conditions. Since the amine of the AA2 is Fmoc protected, this ensures that only one coupling reaction between the free amine of the first amino acid and the carboxylate of the second amino acid can occur. This prevents any unwanted elongation and allows a peptide chain of specific sequence to be synthesized.

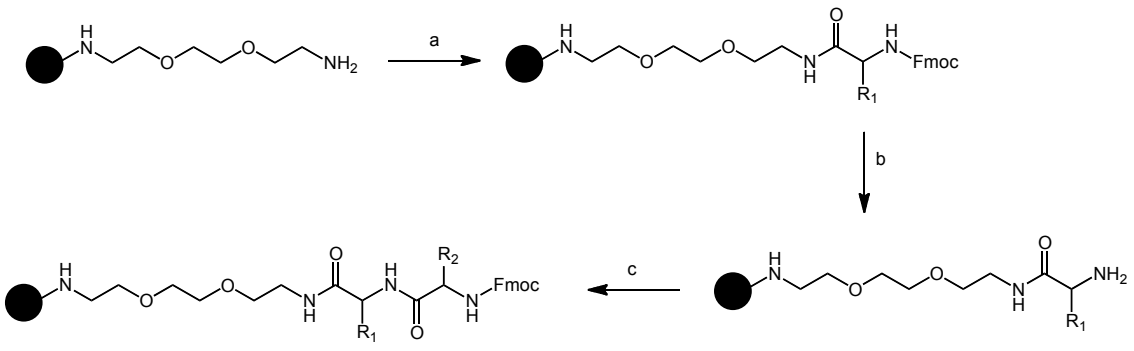

Scheme 2.1: General SPPS protocol. Reagents and conditions: a) AA1, HBTU, DIPEA, DMF, shaken 1 h at RT. b) 20 % piperidine in DMF, 7 min x 3. c) AA2, HBTU, DIPEA, DMF, shaken 1 h at RT.

2.1.2 Resin and Linker Options

Prior to beginning the synthesis of LLP2A, one must choose an appropriate solid phase resin. There are numerous solid phase resins available to meet the requirements of specialized synthesis. For this project, the solid phase target needs to be cleaved from the resin without the use of strong acid, as this would prematurely remove the *t*-butyl protecting group on the side-chain carboxylic acid of the 2-amino adipic acid (Aad) residue. This would permit unwanted chemistry to occur at this position during the conjugation of the imaging and peptide moieties. Self-polymerization and/or cyclization of LLP2A could occur between the free side chain carboxylate of one LLP2A and the free terminal amine of the same or another molecule of LLP2A, resulting in a biologically inactive species. Therefore the *t*-butyl protecting group must be cleaved only once the imaging moiety has been conjugated to LLP2A. A base labile resin would not be orthogonal with the proposed Fmoc synthetic strategy, as part of the synthetic strategy employs DIPEA during coupling reactions and removal of Fmoc with piperidine (Scheme 2.1), both of which could inadvertently cleave the peptide from a base labile resin. Therefore, a resin that can be cleaved though use of mild acid would be appropriate for this synthesis.

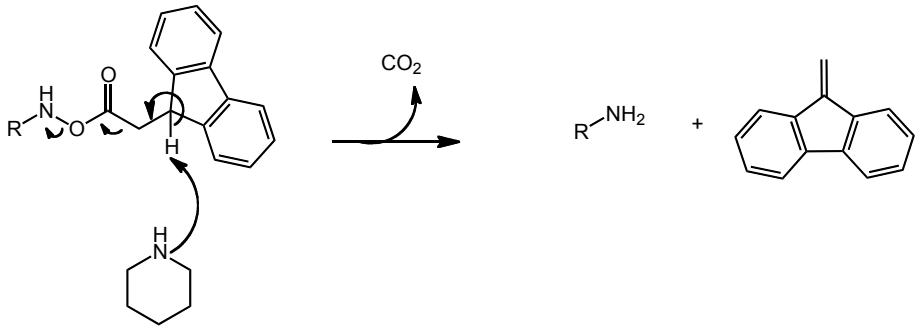

Scheme 2.2: Deprotection of Fmoc under basic conditions to afford a free amine.

SPPS resins are often available with a linker pre-attached since many peptide projects require the use of a linker. For the purposes of this project, the linker must fulfill the following criteria: 1) allow for solubility under physiological conditions and have low toxicity; and 2) be a sufficient length in order to distance the imaging moiety from the peptide so that it does not affect the peptide's receptor-binding abilities. Many commonly used linkers in bioconjugate chemistry are composed of ethylene glycol units. Ethylene glycol affords the required low toxicity and the oxygens allow increased hydrophilicity to maximize solubility in biological systems. An ethylene glycol unit that is functionalized at both ends with a free amine would enable SPPS at one end and facile imaging moiety conjugation at the other. As such, an O-bis-(aminoethyl)ethylene glycol linker was hypothesized to meet the criteria outlined above.

A polystyrene-based trityl-functionalized resin allows cleavage of products through reaction with HFIP, a weak acid. Exposure to HFIP would cleave the resin-peptide bond, yet be mild enough to leave any other acid-labile protecting groups intact. Combining this trityl resin with the aforementioned linker would provide a starting point for the SPPS of LLP2A (Figure 2.1). This resin was purchased preloaded with the linker moiety.

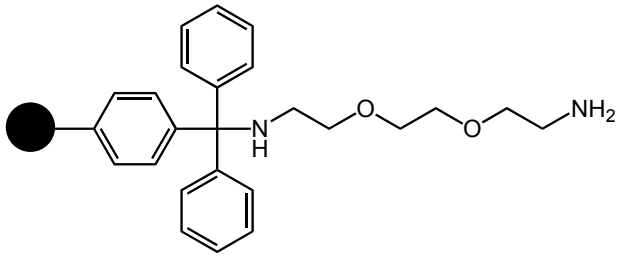

Figure 2.1: O-bis-(aminoethyl)ethylene glycol trityl resin to be used in the SPPS of LLP2A.

2.1.3 Peptide Coupling Reagents

There are several reagents available to form amide bonds from amines and carboxylic acids. The unaided nucleophilic attack of the amine on the carbonyl is too slow to be of any synthetic use, thus activating groups are routinely added to the reaction to increase the rate. Carbodiimides are commonly used in peptide coupling; these react with the carboxylate of the amino acid to create a good leaving group. First a base, typically DIPEA, deprotonates the carboxylic acid of the amino acid, which can then act as a nucleophile and attack the central carbon of the carbodiimide. This yields an O-acyl urea, which is an activated ester. Subsequent nucleophilic attack by the free amine of the other amino acid on the O-acyl urea yields the desired peptide bond, as well as the urea byproduct. The most popular carbodiimide coupling reagents are DCC, DIC, and EDC (Figure 2.2).

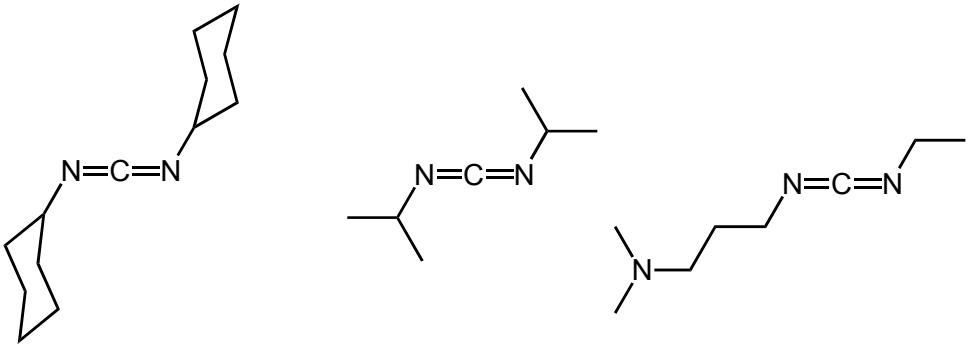

Figure 2.2: Structures of DCC, DIC, and EDC coupling reagents.

The wide variety of coupling agents that accomplish the same end goal, amide bond formation, allows the user to choose the reagent best suited for the task at hand.

DCC is most useful for solution phase coupling, as the urea byproduct is highly insoluble in nearly all organic solvents. DIC and EDC are generally preferred for SPPS, since their urea byproducts are soluble in a variety of solvents, allowing facile removal of these species by filtration. The high reactivity of the O-acyl urea intermediate can sometimes lead to racemization and/or transfer of the acyl group to an adjacent nitrogen on the carbodiimide. In order to limit this, HOBt can be introduced into the reaction. This will attack the O-acyl urea before the free amine of the other amino acid, forming another less reactive O-acyl urea that suppresses racemization and eliminates the possibility of acyl transfer. The free amine then attacks this species and the amide bond is formed, ejecting the HOBt molecule, which can undergo further reaction.

Ongoing developments in peptide synthesis have yielded coupling reagents that bypass the addition of a carbodiimide. Here, HBTU, or a derivative thereof, is added as the salt of a non-nucleophilic anion. Available reagents include HBTU, HATU, and HCTU, pictured below in Figure 2.3. For the purposes of this project, HBTU was the coupling reagent of choice due to its relatively high coupling yield and cost effectiveness.

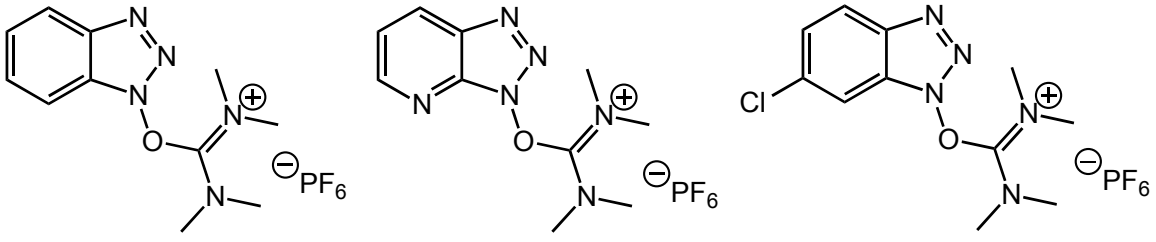

Figure 2.3: Structures of coupling reagents, from left to right: HBTU, HATU, and HCTU.

2.2 Solid Phase Peptide Synthesis of LLP2A

The beginning of the SPPS of LLP2A involves the loading of the resin with Fmoc-Ach-OH. The coupling of the first amino acid to the resin is a crucial step in the synthesis of any peptide. Without complete loading, the second amino acid in the sequence may be inadvertently attached directly to the resin during the subsequent coupling reaction. This results in the formation of an incomplete peptide that will likely have no or limited biological activity. In order to maximize yield of the desired peptide, it is advantageous to ensure complete loading of the first amino acid prior to the subsequent reaction.

Resin swelling contributes to achieving overall resin loading. Prior to use, solid phase resins must be swollen in the appropriate solvent that permits the resin to expand. Insufficient swelling can cause poor reaction site accessibility and diminished reaction rates[45] since the reactive sites are not in an available position to undergo reaction. Testing revealed that swelling for two hours was enough to allow complete loading, with additional swelling time yielding no increase in loading. Thus, in the SPPS of LLP2A, the resin was swollen in DCM for two hours with occasional stirring prior to the addition of any reagents.

After swelling, the solvent was removed from the resin by filtration. The design of the reaction vessel, a 10 mL plastic tube (also called a spin column) with a frit at the bottom, allows for simple suction filtration enabling the resin to remain in the same vessel for the duration of the synthesis. The reactants were then added to the vessel, which included Fmoc-Ach-OH, HBTU, DIPEA and DMF (Scheme 2.3). The reaction vessel was then capped at both ends and shaken gently for one hour. As another precaution

to ensure complete loading, four equivalents of the amino acid and coupling reagent are added to the resin during all coupling reactions.

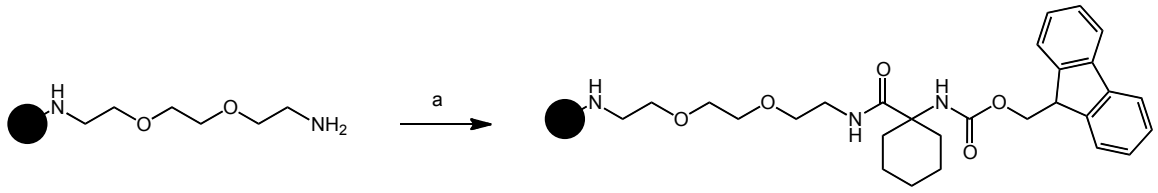

resin 1

Scheme 2.3: Installment of Fmoc-Ach-OH onto the resin. Reagents and conditions: a) Fmoc-Ach-OH, HBTU, DIPEA, DMF shaken 1 h at RT.

The time of reaction is also important. If the reaction time is too short, incomplete loading may be observed. However, if the reaction time is too long, there may be removal of the base-labile Fmoc protecting group by DIPEA and an undesirable double coupling reaction at the deprotected terminal amine site. Through experimentation, it was determined that a coupling reaction time of one hour using HBTU provided complete coupling without elongation and this method was used throughout the SPPS portion of this project. After the reaction was complete, the solution was removed by filtration. The resin was washed thoroughly with DMF and DCM in order to remove any remaining reactants and reagents.

After the installment of the first amino acid, 1-(Fmoc-amino)cyclohexanecarboxylic acid (Fmoc-Ach-OH), the loading of the resin was quantified so that the required amount of amino acid for subsequent couplings could be calculated. This is done by observing the amount of Fmoc deprotection product,

dibenzofulvene (DBF), produced from a known mass of dry resin. While routine Fmoc deprotection will employ piperidine as a base, 1,8-diazabicycloundec-7-ene (DBU) is used for resin loading determination (Scheme 2.4). Use of a nucleophilic base, such as piperidine, will cause deprotection of the Fmoc to yield not only DBF, but also forming the DBF-piperidine adduct. This may cause varying UV absorption, depending on the equilibrium between DBF and the DBF-piperidine adduct. Thus, the non-nucleophilic sterically encumbered base DBU is used instead since it will not form an adduct with DBF. The amount of DBF liberated in the reaction will be stoichiometric with the amount of Fmoc present on the resin and permit accurate loading quantification.

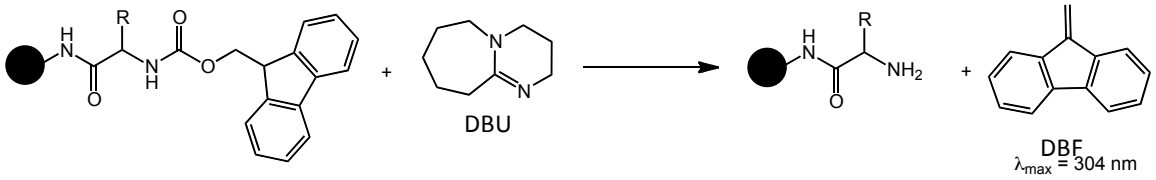

Scheme 2.4: Reaction of DBU with Fmoc to produce DBF, allowing quantification of resin loading.

A small amount of the resin at the tip of a spatula, approximately 15 mg, was removed and dried under vacuum for 12 hours to remove any solvent which would add extra mass that may be incorrectly attributed to the resin. Two separate vials each containing a precise mass (approximately 6 mg each) of dried resin were then prepared. The addition of 2 mL of a 2 % DBU in DMF solution allows complete cleavage of the Fmoc protecting group from the resin, yielding DBF. Two serial dilutions are then made with ACN. A blank solution is prepared in the same way, omitting the resin. The

solutions are then analyzed with UV-Visible spectroscopy at 304 nm, the λ_{max} for DBF. After determining the absorbance, the molar absorbtivity of DBF (7624 $M^{-1}cm^{-1}$) is then used to calculate the concentration. This allows for a final measurement of Fmoc quantity in mmol/g resin, thus quantifying the amount of amino acid that has been coupled onto the resin.

What is considered to be "full loading" varies by resin, and also differs between batches of the same resin. For the O-bis-(aminoethyl)ethylene glycol trityl resin, complete loading can be anywhere from 0.3 – 1.0 mmol/g according to the manufacturer. After installation of the Fmoc-Ach-OH residue, the loading was determined to be 0.47 mmol/g. This is a reasonable loading value and a Kaiser test can be used to check for free amines and confirm complete loading. The test involves the addition of a ninhydrin solution to the resin. If any free amines are present they will undergo a reaction with the ninhydrin molecules to yield a strong blue color. When the test is performed and no blue color is observed, it can be concluded that there are no free amines and complete coupling has taken place. A Kaiser test was used to confirm there were no free amines on the resin, verifying full loading, and **resin 1** (Scheme 2.3) was acquired.

The next step involves the coupling of Fmoc-Aad(*t*Bu)-OH (Scheme 2.5). The resin was first washed with a piperidine solution (20 % in DMF) for 10 minutes to deprotect the Fmoc group. The solution was then drained from the reaction vessel, and this process repeated twice more. The removal of the Fmoc group could be followed by TLC, as DBF is strongly UV active due to the highly conjugated system. The resin was

then washed thoroughly with DMF to remove any residual piperidine. Lingering piperidine could possibly lead to deprotection of Fmoc-Aad(*t*Bu)-OH and a double coupling to form a Fmoc-Aad(*t*Bu)-Aad(*t*Bu)-OH dipeptide *in situ* which could link with the Ach residue. Mixed in a vial and added to the resin were Fmoc-Aad(*t*Bu)-OH, HBTU, DIPEA and DMF. The reaction was shaken for 1 hour, then drained and washed with DMF and DCM.

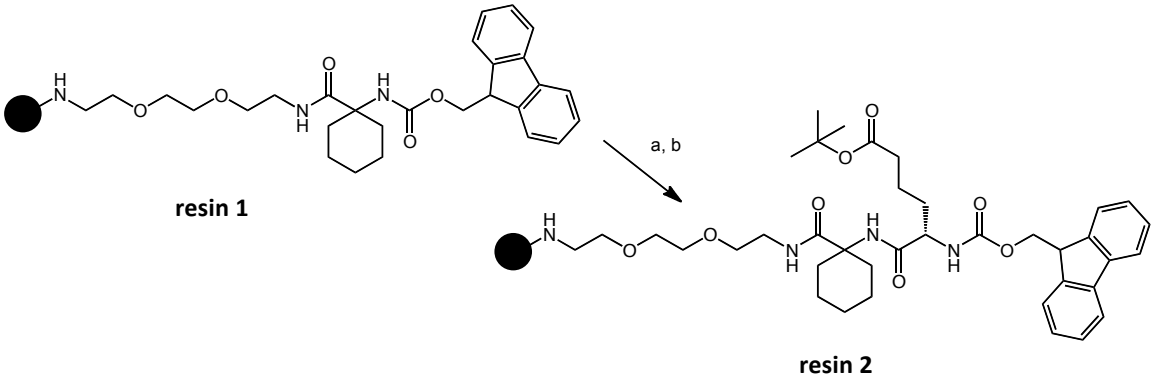

Scheme 2.5: Removal of Fmoc protecting group of **resin 1** and coupling of Fmoc-Aad(*t*Bu)-OH onto Ach. Reagents and conditions: a) 20 % piperidine in DMF, 10 min at RT. Repeated twice more. b) Fmoc-Aad(*t*Bu)-OH, HBTU, DIPEA, DMF shaken 1 h at RT.

Unfortunately, it was at this point in the synthesis where difficulties were encountered. Testing showed that no amino acid had been coupled onto the free amine of the Ach residue. A Kaiser test was positive for free amines. A small portion of the resin was cleaved and investigated by mass spectrometry, which did not indicate the presence of the desired product. Confused by the failure of this normally robust reaction, the starting material was investigated. Analysis of Fmoc-Aad(*t*Bu)-OH by mass

spectrometry and ^{1}H NMR showed neither the expected mass nor any expected proton signals. Thus, it was found the starting material was not as advertised and in fact appeared to be some type of inorganic compound. Further inquiry with the vendor could not explain this phenomenon, and new product was shipped.

The new product was tested prior to use and the results were in agreement with the data provided by the supplier. The synthesis was started anew, with the installation of Fmoc-Ach-OH on fresh resin. Subsequent coupling with Fmoc-Aad(*t*Bu)-OH yielded the desired product, as shown by mass spectrometry. The mass spectrum did not indicate the presence of a truncate, however, a Kaiser test indicated the presence of free amines. It was hypothesized that although the new batch of amino acid did in fact contain Fmoc-Aad(*t*Bu)-OH, it was perhaps not pure by mass. A second coupling reaction could be done, however this risks the formation of an unwanted elongation of the peptide. At this point, due to time constraints, it was decided to move forward with the synthesis and deal with any future purification that may be necessary.

After removal of the Fmoc protecting group by washing with a 20 % solution of piperidine in DMF, a solution of Fmoc-Lys(Dde)-OH, HBTU, DIPEA and DMF was added to the resin (Scheme 2.6). The reaction was shaken gently for 1 hour and the solution was removed by filtration. Mass spectrometry analysis showed the presence of the product and a Kaiser test was negative for free amines.

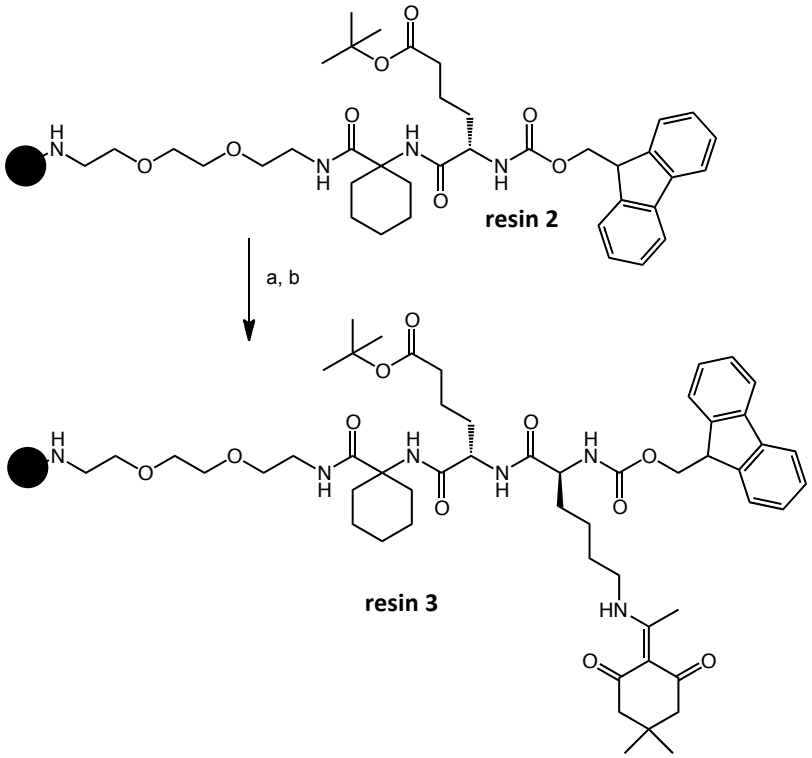

Scheme 2.6: Removal of Fmoc protecting group of **resin 2** and coupling of Fmoc-Lys(Dde)-OH onto Aad. Reagents and conditions: a) 20 % piperidine in DMF, 10 min at RT. Repeated twice more. b) Fmoc-Lys(Dde)-OH, HBTU, DIPEA, DMF shaken 1 h at RT.

With the tripeptide now in hand, the next step involves the coupling of the terminal 2-(4-(3-*o*-tolylureido)phenyl)acetic acid **1**, which must first be synthesized in solution (Scheme 2.7). This synthesis involves the carbamide-forming condensation of 4-aminophenyl acetic acid and *o*-tosyl isocyanate. 4-Aminophenyl acetic acid was dissolved in DMF and added dropwise into a stirring solution of *o*-tosyl isocyanate in DMF. After stirring for 2 hours, the solvent volume was reduced and the reaction was poured onto ethyl acetate. This resulted in a coffee coloured precipitate. The mixture

was then filtered and the precipitate was characterized by ^{1}H NMR and MS with no further purification required.

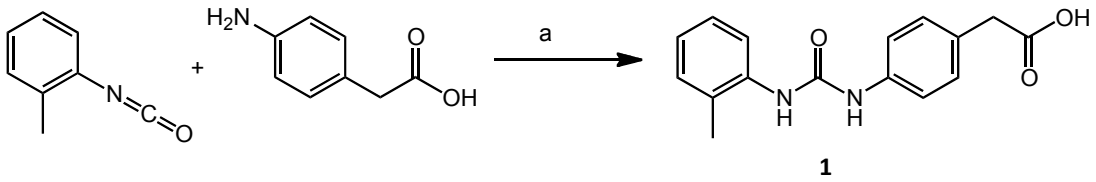

1

Scheme 2.7: Synthesis of 2-(4-(3-*o*-tolylureido)phenyl)acetic acid. Reactions and conditions: a) DMF, stirred at RT for 2 hours.

With this product in hand, the Fmoc protecting group was removed from **resin 3** by washing three times with 20 % piperidine in DMF. A solution of 2-(4-(3-*o*-tolylureido)phenyl)acetic acid, HBTU, DIPEA and DMF was added to the resin and the vessel was shaken for 1 hour (Scheme 2.8). Another coupling reaction was performed with half the equivalents used previously since there was no risk of peptide elongation due to the absence of an N-terminus on the 2-(4-(3-*o*-tolylureido)phenyl)acetic acid. After filtration to remove the solvent, the resin was washed with DMF and DCM. Following analysis revealed the reaction was successful, with the corresponding product peak observed in the mass spectrum.

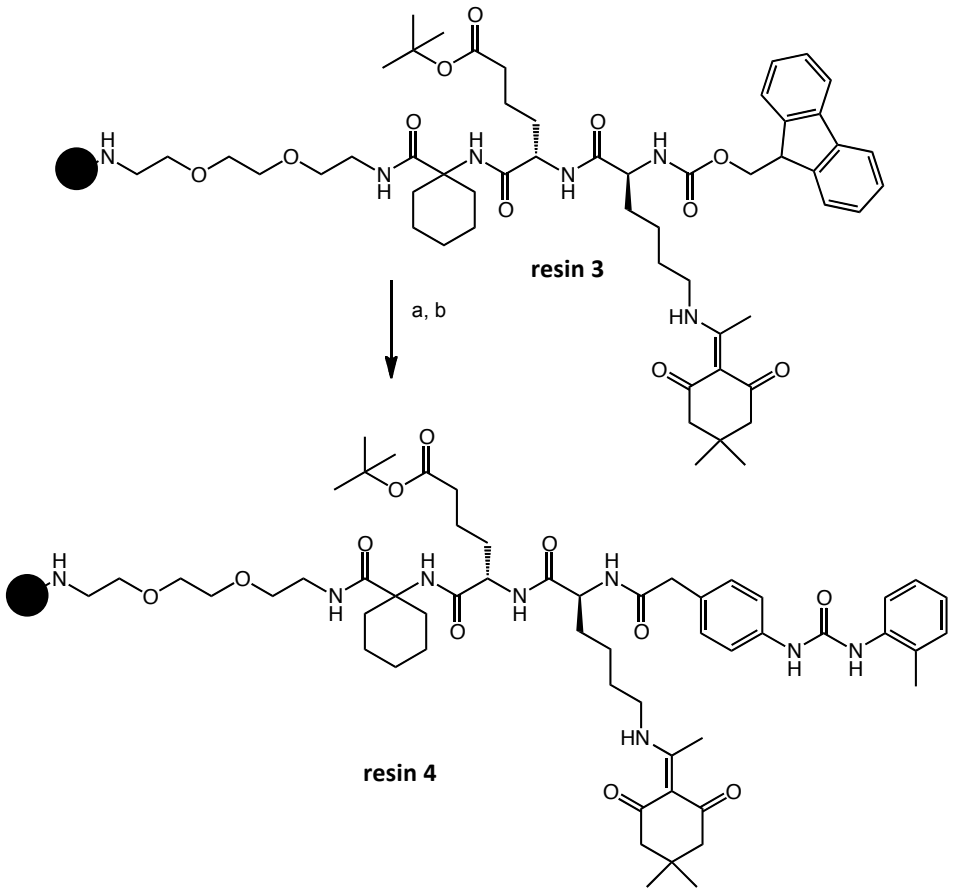

Scheme 2.8: Removal of Fmoc protecting group of **resin 3** and coupling of 2-(4-(3-*o*-tolylureido) phenyl)acetic acid onto Lys. Reagents and conditions: a) 20 % piperidine in DMF, 10 min at RT. Repeated twice more. b) 2-(4-(3-*o*-tolylureido)phenyl)acetic acid, HBTU, DIPEA, DMF shaken 1 h at RT.

The final step in the SPPS of LLP2A is the coupling of 3-(3-pyridyl)acrylic acid onto the side chain of the lysine residue (Scheme 2.9). Before this can be done, the Dde group must be deprotected. Dde is an excellent protecting group for side chain amines because it is completely orthogonal with both acid and base treatments. Dde is deprotected by washing with a solution of 2 % hydrazine in DMF. Following deprotection, a solution of 3-(3-pyridyl)acrylic acid, HBTU, DIPEA and DMF was added.

The vessel was shaken for 1 hour and the solution was filtered off and the resin washed with DMF. This completes the SPPS of LLP2A.

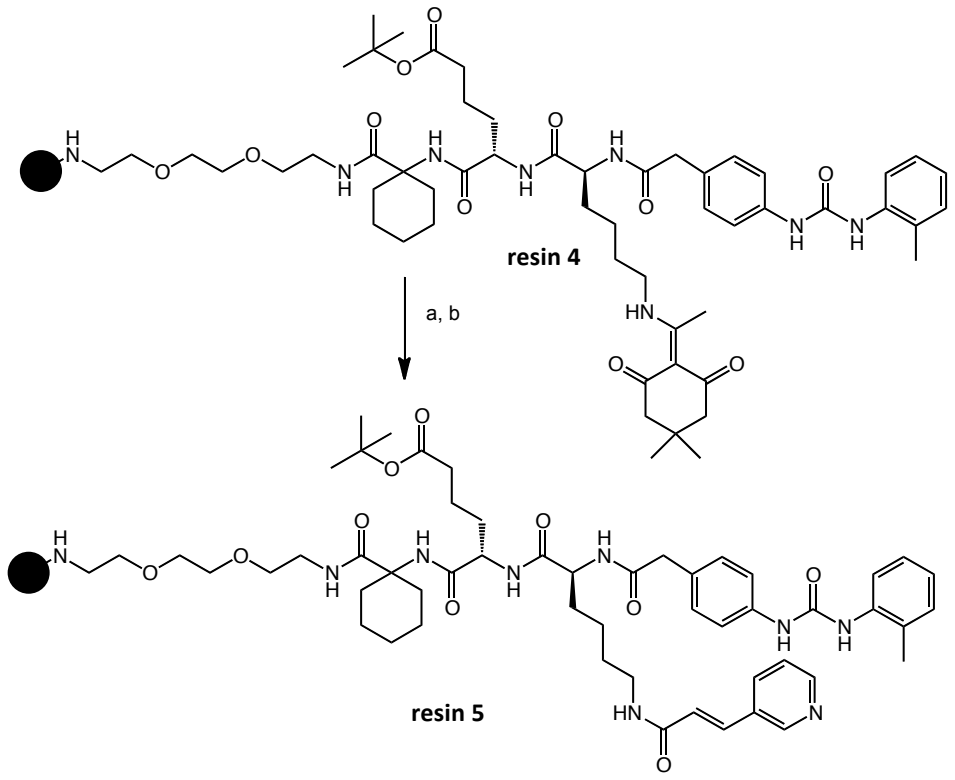

Scheme 2.9: Removal of Dde protecting group of **resin 4** and coupling of 3-(3-pyridyl)acrylic acid onto the side chain of Lys. Reagents and conditions: a) 2 % hydrazine in DMF, 4 min at RT. Repeated twice more. b) 3-(3-pyridyl)acrylic acid, HBTU, DIPEA, DMF shaken 1 h at RT.

The complete peptide could now be cleaved from the resin (Scheme 2.10). After placing **resin 5** in a round bottom flask, a solution of 30 % HFIP in DCM was added. Immediately, the resin turned a bright orange colour, indicating the presence of a trityl cation and that the product had been liberated from the resin. The reaction was gently stirred for 30 minutes to ensure that all peptide had been cleaved; the orange colour faded during this time. The resin was filtered off, with the desired product now

dissolved the filtrate. The filtrate volume was reduced and the product, LLP2A(*t*Bu), was precipitated as a fluffy, white solid using diethyl ether.

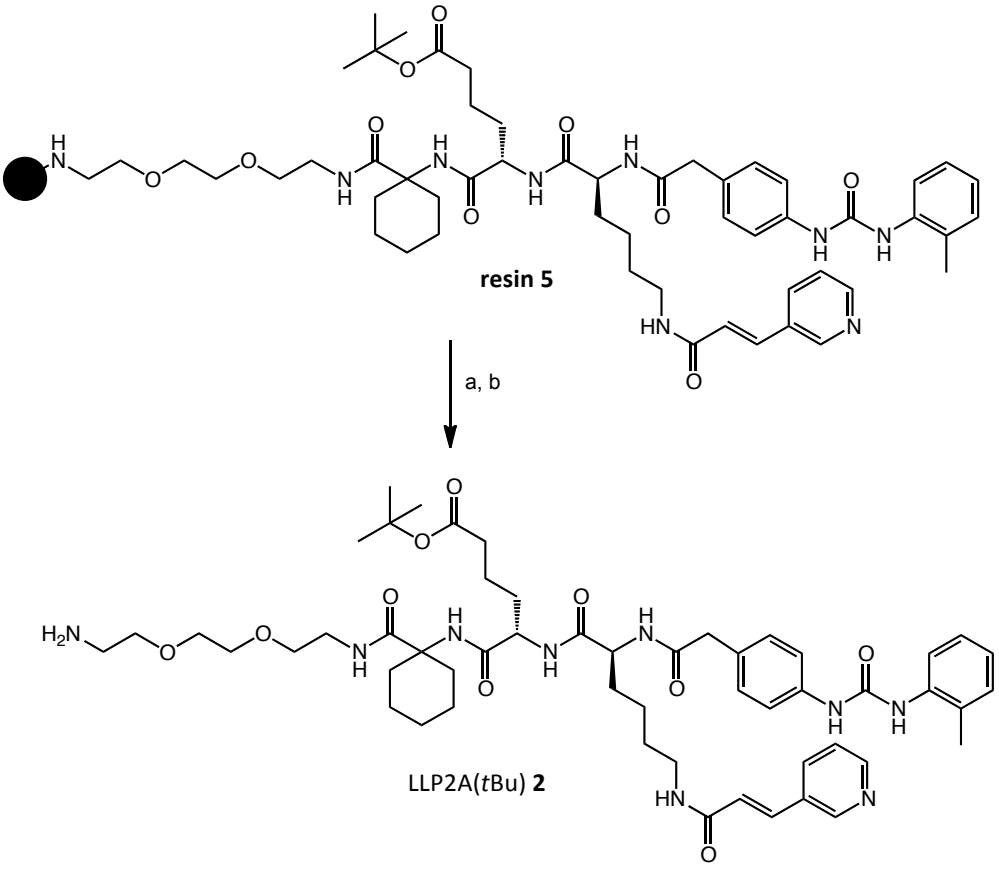

Scheme 2.10: Cleavage of **resin 5** to produce LLP2A(*t*Bu) **2**. Reagents and conditions: a) 30 % HFIP in DCM, 30 min at RT. b) diethyl ether.

At this point, the precipitate was analyzed for purity. The mass spectrum revealed the corresponding [M+H$^+$] peak of 999, however, a peak of 799 was also observed. This undesired peak indicated the presence of a truncate. As a result of previous experimentation, it was suspected that complete coupling of the Aad(*t*Bu) residue may not have occurred. The corresponding mass of Aad(*t*Bu) is 200 g/mol, confirming it to be the residue absent in this truncation. The ratio of truncate to

LLP2A(*t*Bu) was investigated by RP-HPLC (Figure 2.4). A clean trace was produced, consisting of one peak at 8 minutes and one at 12 minutes. These peaks were collected and their masses were analyzed, indicating that the second peak was LLP2A(*t*Bu), and the first peak was the truncate. The areas of these peaks suggest that the truncate was approximately 20 % of the product.

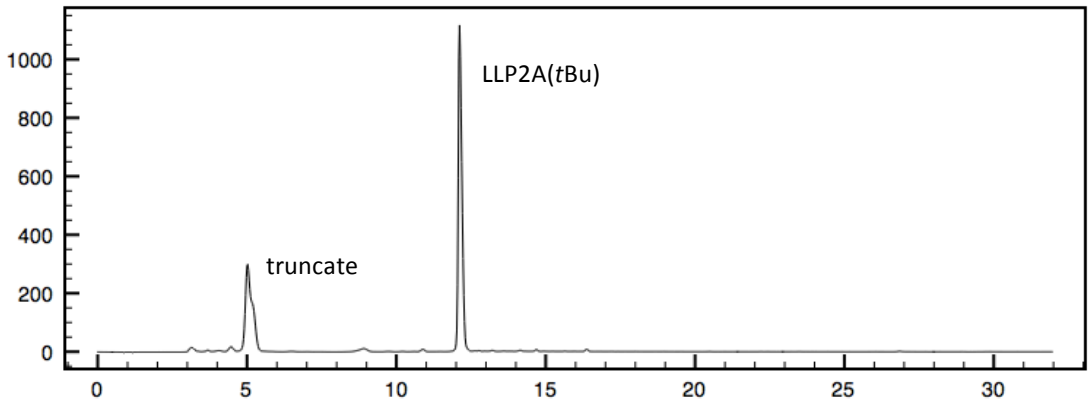

Figure 2.4: RP-HPLC trace of LLP2A(*t*Bu) and truncate.

Preparative TLC was used to purify the desired product from the truncate. Using a 10 % NH_4OH in EtOH solution, the truncate and LLP2A(*t*Bu) could be resolved on TLC, with LLP2A(*t*Bu) running slightly higher on the plate. The strongly absorbing aromatic residues allowed visualization with a handheld UV lamp. The corresponding spot was scraped off of the glass plate and MeOH was added to the remove the product. The mixture was vortexed and then centrifuged. The solvent was then removed and this process was repeated twice more. Complete removal of the product could be followed with UV lamp, as the silica would not exhibit the dark colour characteristic of a UV

absorbing compound once the entire product had been removed. The volume of the solution was then reduced under vacuum and the product was precipitated via addition of diethyl ether. This product was further analyzed with RP-HPLC to confirm its purity, as shown in Figure 2.5.

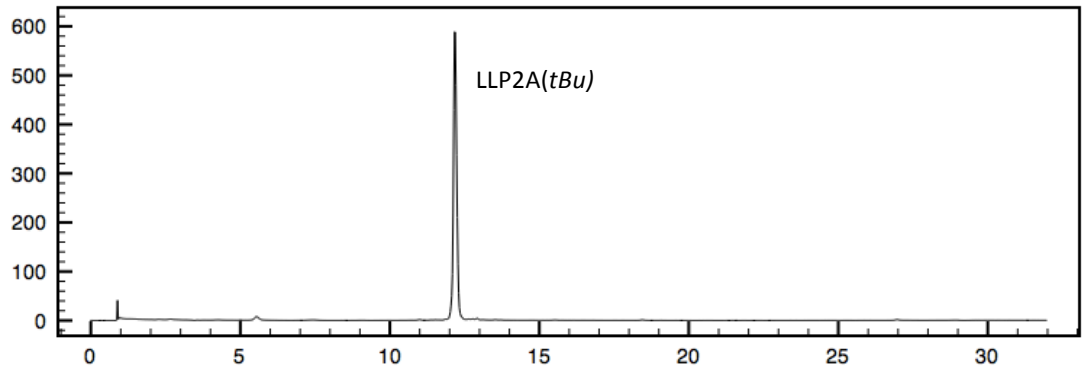

Figure 2.5: RP-HPLC trace of purified LLP2A(*t*Bu).

2.3 Solution Phase Synthesis and Conjugation to LLP2A

2.3.1 Synthesis of ArB(OR)$_2$-LLP2A

With the biologically active portion of the target compound complete, it could now be functionalized to allow imaging studies to take place. This is conveniently done through acylation of the terminal free amine of the LLP2A(*t*Bu). Conjugation to a compound containing a protected boronic acid will enable direct, one-step radiolabeling of the peptide. Alternatively, functionalizing the LLP2A with an azide will allow for conjugation to any number of functional groups through facile click chemistry.[27]

To this end, 2,4,6-trifluoro-3-(4,4,5,5-tetraphenyl-1,3,2-dioxaborolan-2-yl)benzoic acid (referred to as $ArB(OR)_2$) was synthesized (Scheme 2.11). The starting material, 2,4,6-trifluorobenzoic acid, is first deprotonated by adding two equivalents of *n*-butyl lithium while at -78 °C. The first equivalent deprotonates the carboxylic acid, while the second equivalent deprotonates one of the equivalent aromatic hydrogens resulting in a vivid orange-red colour. At this point, trimethyl borate is added to the reaction and there is nucleophilic attack by the carbanion on the empty p orbital of the boron. After 15 minutes, the reaction was quenched using HCl and allowed to warm to room temperature. 1,1,2,2-Tetraphenyl pinacol was then added, displacing the methoxy groups on the boron and producing methanol. The product was then isolated by column chromatography using an ethyl acetate and hexane solvent system.

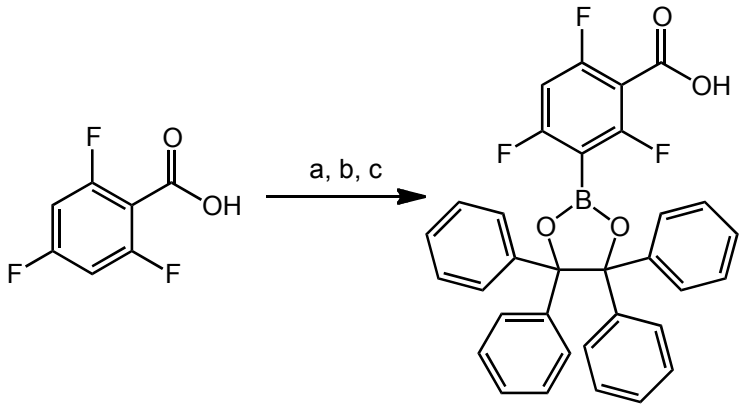

3

Scheme 2.11: Synthesis of $ArB(OR)_2$ **3**. Reagents and conditions: a) 2,4,6-trifluorobenzoic acid, THF, *n*-BuLi at -78 °C for 2 hours. b) trimethyl borate, THF, 2 hours at RT. c) HCl, 1,1,2,2-tetraphenyl pinacol, THF, 2 hours at RT.

The conjugation of the $ArB(OR)_2$ to LLP2A(*t*Bu) was done in similar fashion to the other amide bond forming reactions used during the SPPS portion of the project. EDC, HOBt, pyridine and $ArB(OR)_2$ were added to a solution of LLP2A(*t*Bu) and DMF and the reaction was allowed to continue overnight at RT. The addition of diethyl ether caused a white precipitate to form, which was then be isolated from the solution. The *t*-butyl protecting group on the side chain of Aad was then removed by adding the solid to a 50 % solution of TFA in DCM and stirring for 1 hour. The solvent volume was then reduced and the product precipitated with diethyl ether. The product was isolated by chromatography with 7 % MeOH in DCM, yielding the final target compound, $ArB(OR)_2$-LLP2A.

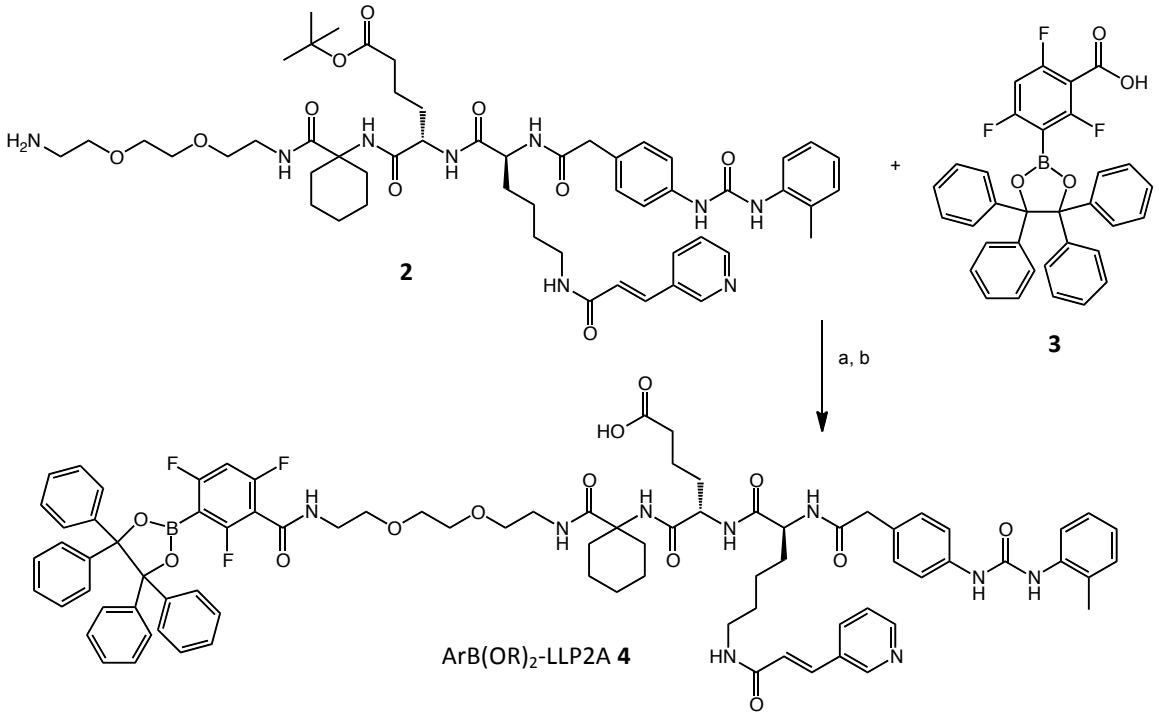

Scheme 2.12: Synthesis of $ArB(OR)_2$-LLP2A **4**. Reagents and conditions: a) $ArB(OR)_2$, LLP2A(*t*Bu), EDC, HOBt, pyridine, THF stirred for 16 hour at RT. b) TFA in DCM stirred for 1 hour at RT.

2.3.2 Synthesis of N_3-LLP2A

In order to prepare LLP2A for click chemistry, the peptide must be functionalized with an azide to allow reaction with an alkynyl-modified $ArB(OR)_2$. These two molecules may then be conjugated together through a Huisgen cycloaddition click reaction yielding a 1,2,3-triazole, which is catalyzed by copper(I). It was decided that 5-azido pentanoic acid[46] would provide a suitable chain length and would allow production from a readily available starting material, ethyl 5-bromo pentanoate. This material was dissolved in DMSO and NaN_3 was added, causing an S_N2 reaction where the N_3 anion displaces the bromide. This product, ethyl 5-azido pentanoate, was then extracted into diethyl ether. The ester was cleaved by addition of 1N NaOH solution at RT, stirring overnight. The solution was then acidified with concentrated HCl and the product was again extracted into diethyl ether. After removing the solvent, a yellow oil was produced. The synthesis could be followed with ^1H NMR. The shift in the methylene peaks after installation of the N_3 group, as well as the absence of the ethyl peaks following ester hydrolysis served as good indicators of successful synthesis.

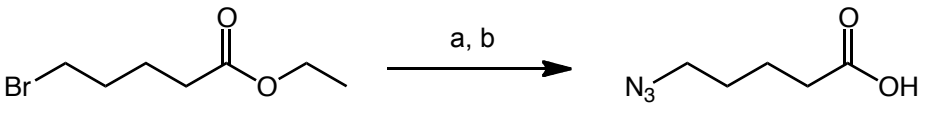

5

Scheme 2.13: Synthesis of 5-azido pentanoic acid **5**. Reagents and conditions: a) Ethyl 5-bromo pentanoate, sodium azide, DMSO stirred for 12 hours at RT. b) NaOH, stirred for 12 hours at RT.

With this product in hand, it was now possible to acylate the LLP2A(*t*Bu) and create the "clickable" LLP2A ligand. The peptide bond between 5-azido pentanoic acid and LLP2A(*t*Bu) was formed using HBTU and DIPEA in DMF. The reaction proceeded for 1 hour, after which the solvent was reduced and the product precipitated with diethyl ether. The precipitate was added to a 50 % solution of TFA in DCM to remove the *t*-butyl protecting group on the Aad residue since the carboxylate cannot participate in the click reaction to conjugate an alkynyl-$ArBF_3$. After stirring for 1 hour, the solvent was reduced under vacuum and the product precipitated with diethyl ether, yielding a white solid that was purified by RP-HPLC.

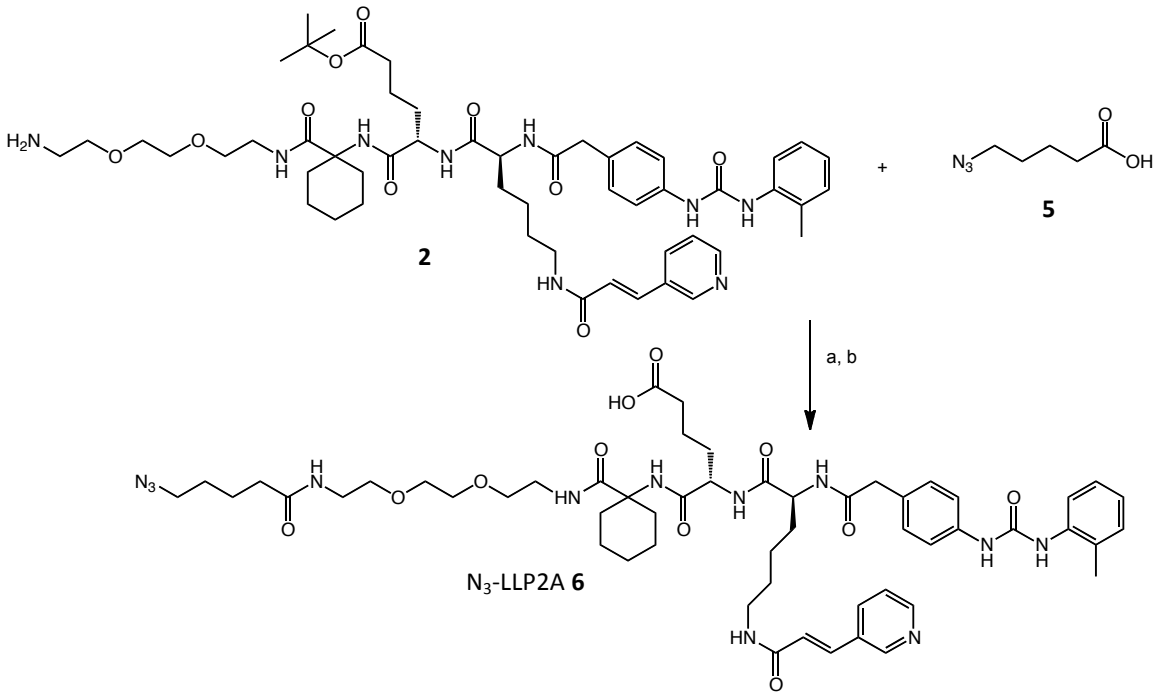

Scheme 2.14: Synthesis of N_3-LLP2A **6**. Reagents and conditions: a) 5-azido pentanoic acid **5**, LLP2A(*t*Bu), HBTU, DIPEA, THF stirred for 1 hour at RT. b) TFA in DCM stirred for 1 hour at RT.

2.4 Cold Fluorination of $ArB(OR)_2$-LLP2A

2.4.1 Perspectives on $ArBF_3$ Formation

Now that the $ArB(OR)_2$-LLP2A had been synthesized, fluorination experiments could be conducted. Two fluorination methods are possible: 1) slow fluorination (~12 hours) under very mildly acidic conditions (pH 3-4) for relatively large-scale production of $ArBF_3$-LLP2A; and 2) fast fluorination (< 1 hour) under quite acidic (pH < 2) conditions for imaging-scale production. For PET imaging purposes, fluorination needs to be fast in order to minimize the amount of decay that occurs during labeling and/or prior to the drug reaching the patient. Unfortunately, fast fluorination to simulate radiolabeling of $ArB(OR)_2$s requires rather acidic conditions to increase the rate of removal of the boronic acid protecting group. This low pH also increases the possibility that the peptide may be altered or cleaved in some way during the fluorination reaction. However, slow fluorination necessitates only mildly acidic conditions, allowing for significant amounts of the $ArBF_3$ to be produced without regard for side reactions. While this is not useful for imaging, this method provides an opportunity for characterization of the fluorinated peptide and *in vitro* cell binding studies. If the products of the slow and fast fluorination are revealed to have the same RP-HPLC profile and mass spectrometry analysis, then it can be presumed that the low pH of the fast fluorination is not altering the peptide and it should retain its imaging abilities.

2.4.2 Slow Fluorination of $ArB(OR)_2$-LLP2A

$ArB(OR)_2$-LLP2A was placed in an Eppendorf vial with THF and KHF_2. This mixture was vortexed and allowed to react overnight at RT. The product was precipitated with diethyl ether. RP-HPLC and mass spectroscopy analysis of the precipitate showed a high conversion to the $ArBF_3$-LLP2A as well as a small amount of deboronylated side product.

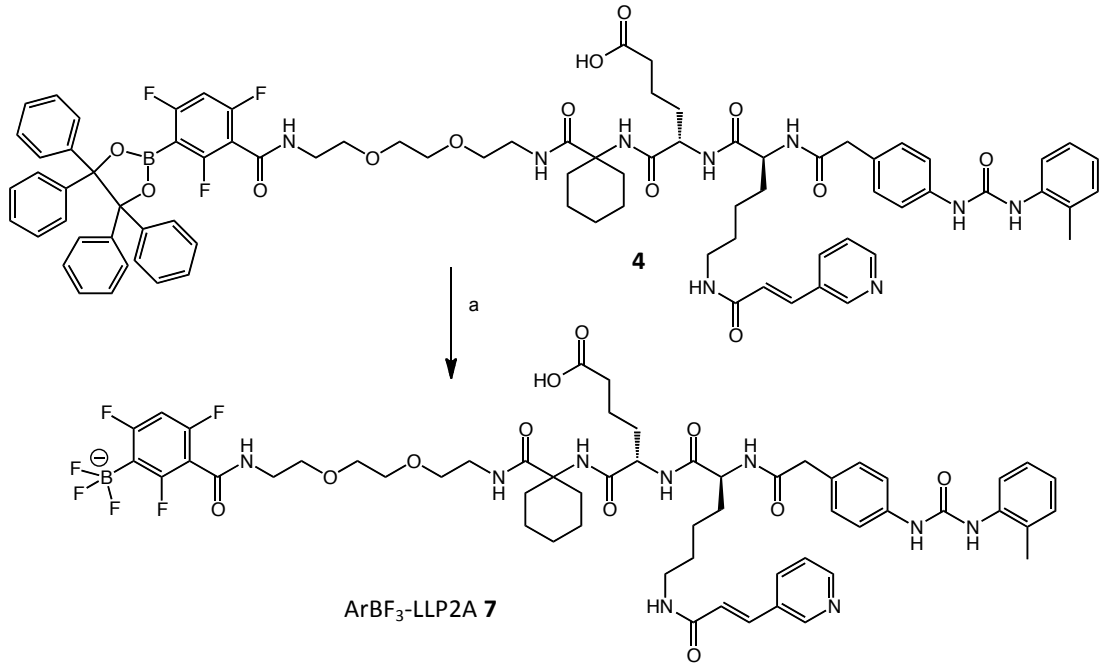

Scheme 2.15: Synthesis of $ArBF_3$-LLP2A **7** by slow fluorination method. Reagents and conditions: a) $ArB(OR)_2$-LLP2A, KHF_2, THF for 12 hours at RT.

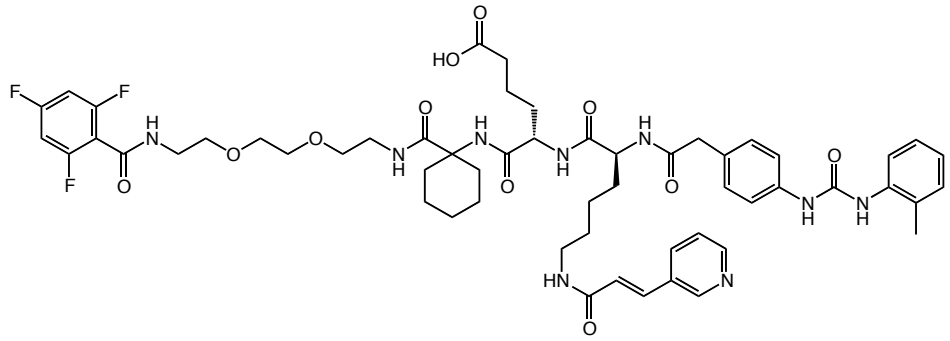

Figure 2.6: Structure of deboronylated side product.

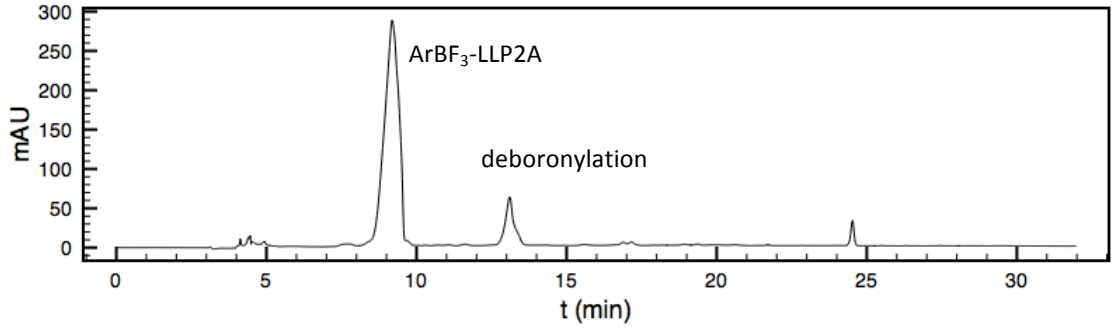

Figure 2.7: RP-HPLC of synthesis of $ArBF_3$-LLP2A by slow fluorination method.

The synthesis of $ArBF_3$-LLP2A can be confirmed through ^{19}F NMR. The $ArB(OR)_2$ will have three peaks, each of integration 1, corresponding to the fluorines on the aryl ring. After fluorination, three peaks of integration 1 as well as a new peak of an integration of 3, representing the 3 fluorides captured as the aryltrifluoroborate, are observed.

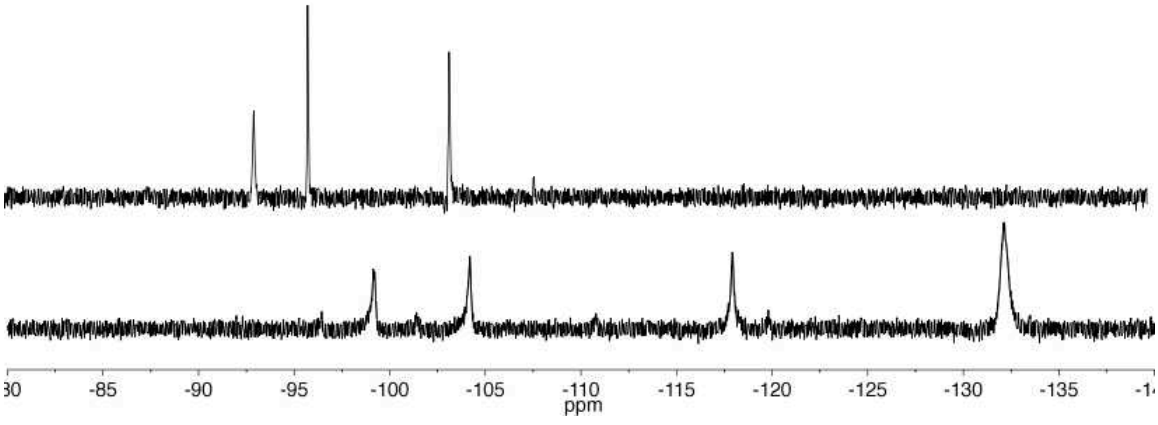

Figure 2.8: ^{19}F NMR of $ArB(OR)_2$ (top) and $ArBF_3$-LLP2A (bottom).

2.4.3 PET Imaging Scale Fast Fluorination of $ArB(OR)_2$-LLP2A

Fast fluorination at low pH using ^{19}F reflects identical conditions that would be used during radiolabeling for *in vivo* PET imaging. Due to the sub-micromole scale of this reaction, characterization by ^{19}F NMR is not an option. However, there is a sufficient amount of product to allow investigation by mass spectrometry and RP-HPLC.

100 Nmol of $ArB(OR)_2$-LLP2A was placed in a small Eppendorf vial and dissolved in 4 µL of THF. 2 µL of 0.125 M $KHF_{2(aq)}$ and 0.5 µL HCl were added and the mixture was vortexed and allowed to sit for 1 hour. The reaction was then quenched with 100 µL of a solution of 5:15:80 NH_4OH:H_2O:EtOH and then analyzed by RP-HPLC. As in the RP-HPLC of the slow method in Figure 2.7, two major peaks were present; the expected $ArBF_3$-LLP2A at 9.18 min and a new peak at 13.17 min. These peaks were collected for mass spectrometry analysis. The identity of the $ArBF_3$-LLP2A was confirmed, and the corresponding mass of the other peak showed it to again be the deboronylation product. The other peaks were not examined further.

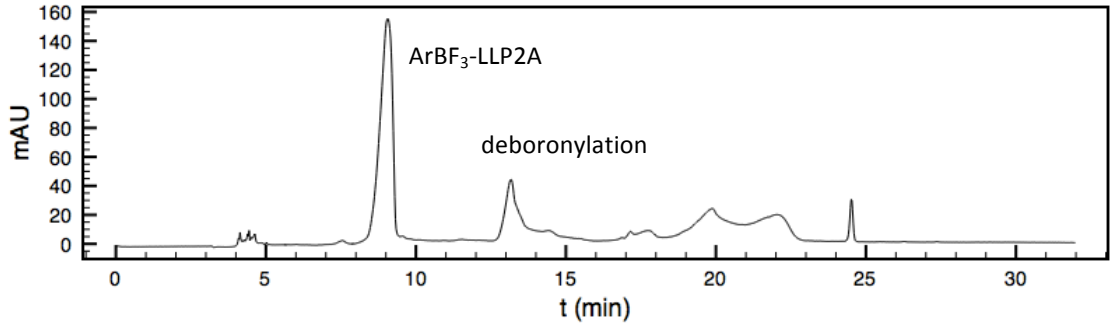

Figure 2.9: RP-HPLC of synthesis of $ArBF_3$-LLP2A by fast fluorination method.

Although the fast method of fluorination also leads to some deboronylation, this byproduct is in low amount. Gratifyingly, there is still a significant amount of $ArBF_3$-LLP2A produced by the fast method, suggesting applicability for PET imaging. It is important to note that the $ArBF_3$-LLP2A is the first peak to elute and that it is distanced from all other peaks, allowing easy isolation by RP-HPLC in a timely manner. In a radiolabeling situation, the quenched reaction would be immediately put onto an RP-HPLC and the pure $ArB^{18}F_3$-LLP2A collected. A sub-ten minute elution time means fast purification resulting in minimal radioactive decay and a high specific activity of the final product.

2.5 Biological Activity Confirmation

2.5.1 Synthesis of FITC-LLP2A

Before the $ArB(OR)_2$-LLP2A can be radiolabeled and tested *in vivo*, it must be shown that the compound is biologically active and binds to cells expressing the $\alpha_4\beta_1$ integrin receptor. To perform a cellular binding assay a fluorescent version of the peptide is required. Of the many fluorescent labeling compounds available, FITC was chosen because it is readily available as the isothiocyanate which makes for facile conjugation to the peptide through thiourea formation. As well, it provides an emission wavelength that is compatible with standard fluorescent microscopy equipment and is economically responsible compared to many other fluorescent compounds. LLP2A(*t*Bu) was added to a solution of 50:50 DMF:Na_2CO_3 buffer and FITC. The reaction was

allowed to proceed for 12 hours at 4 °C and then the product was precipitated with diethyl ether and purified. The *t*-butyl protecting group was then removed by adding it to a solution of 50 % TFA in DCM solution and stirring for 1 hour. Addition of diethyl ether caused a yellow solid to precipitate, after which the solvent was decanted and the product was collected. This compound was purified by TLC prior to *in vitro* studies.

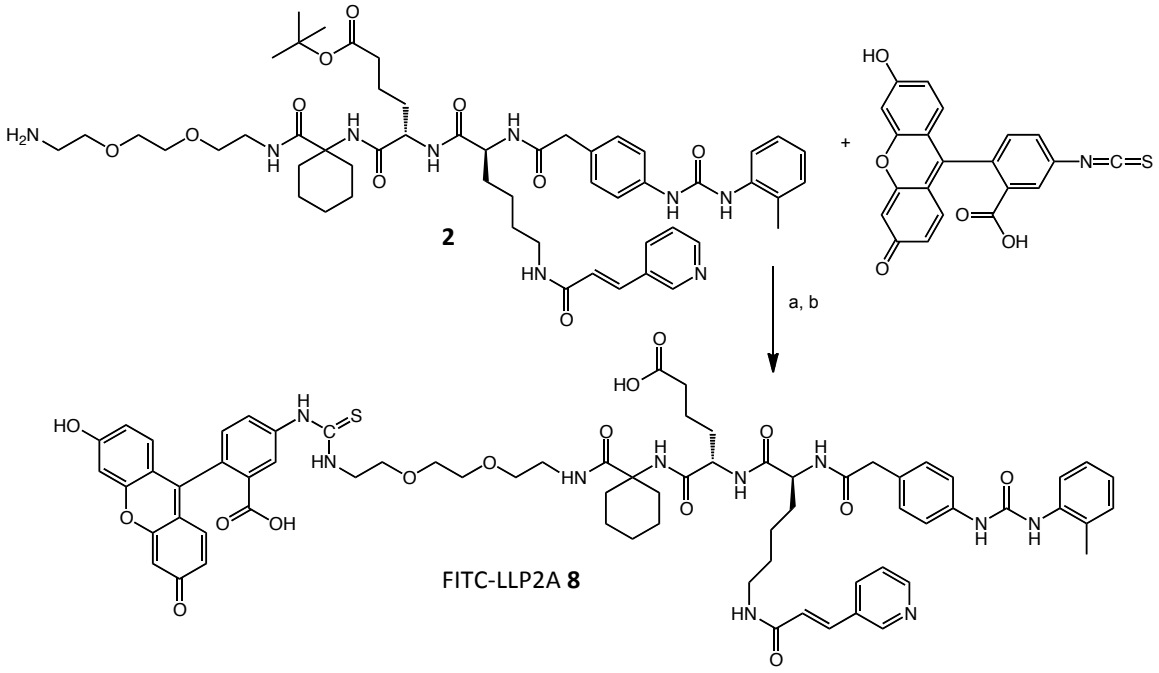

Scheme 2.16: Synthesis of FITC-LLP2A **8**. Reagents and conditions: a) FITC, LLP2A(*t*Bu), 50:50 DMF:Na_2CO_3 buffer stirred for 12 hours at 4 °C. b) TFA in DCM stirred for 1 hour at RT.

2.5.2 Cell Binding Assay

Two experiments were used to confirm the compound's binding activity. FITC-LLP2A binding can be demonstrated by incubating the cells in a buffer containing the

compound. The buffer is removed and then the cells are observed for fluorescence. If the cells exhibit fluorescence, the peptide is bound to the integrin. To further confirm cellular binding, a blocking experiment is then conducted. Fresh cells are first incubated with a non-fluorescent analog of the compound that would be used *in vivo*, in this case, $ArBF_3$-LLP2A. After incubation with $ArBF_3$-LLP2A, the medium is removed and the cells are washed with fresh buffer. The cells are then incubated with FITC-LLP2A for an equal amount of time. This medium is washed away and the cells are examined for fluorescence. A positive binding determination is made if no fluorescence is observed, as the binding sites should be occupied by $ArBF_3$-LLP2A and thus prevent the binding of FITC-LLP2A. With positive results from both of these experiments, the biological activity of the product would be confirmed.

Human MOLT-4 leukemia cells expressing the $\alpha_4\beta_1$ integrin were obtained and proliferated in medium containing 10 mM glucose. The cells were passaged 10 times before being used for binding studies to ensure continuing viability. When enough cells were present, they were split into several batches of approximately 1×10^6 cells each. One aliquot of cells was incubated in TBS buffer containing 400 nM FITC-LLP2A and another aliquot of cells incubated at 1 nM FITC-LLP2A. The TBS buffer also contained 1mM Mn^{2+}, a known activator of the $\alpha_4\beta_1$ integrin.[47, 48] The compound was allowed to bind for 1 hour after which time the cells were centrifuged and the buffer removed. Fresh buffer was added and the cells centrifuged and fresh buffer added once more. This process was repeated again to ensure that no fluorescent compound was left behind that could cause background fluorescence. The cells were then spotted on a

glass plate and examined for fluorescence. Positive results for fluorescence were seen in both the 1 nM and 400 nM concentrations, indicating cellular binding. The results are summarized in Table 2.1 below.

Table 2.1: Results of cell binding fluorescence assay.

Conc. FITC-LLP2A (nM)	Fluorescence observed
1	Yes
400	Yes

a) 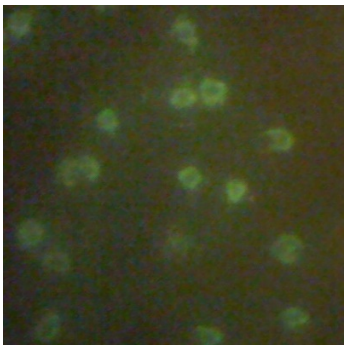 b) 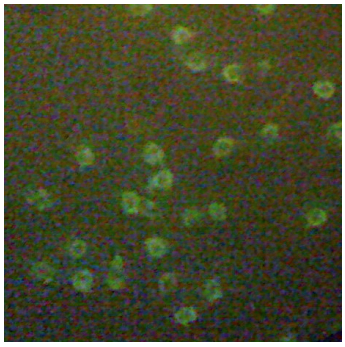

Figure 2.10: MOLT-4 cells exhibiting fluorescence after being treated with (a) 1 nM FITC-LLP2A and (b) 400 nM FITC-LLP2A.

A blocking assay was then preformed. The cells were incubated in TBS buffer (1 mM Mn^{2+}) containing 100 nM $ArBF_3$-LLP2A. The compound was allowed to bind for 1

hour after which time the cells were centrifuged and the buffer removed. Fresh buffer containing either 1 nM or 400 nM FITC-LLP2A was then added and the cells were incubated for 1 hour. The buffer was then washed away and replaced twice to ensure removal of any left over fluorescent peptide, after which the cells were examined for fluorescence. In this case, no fluorescence was observed for both samples. This indicates that the $\alpha_4\beta_1$ integrin binding sites were occupied during the first incubation with $ArBF_3$-LLP2A, preventing the binding of FITC-LLP2A. The results of the two cell binding assays indicate that the compound of interest, $ArBF_3$-LLP2A, is biologically active and will bind *in vivo* to cancer cells expressing the $\alpha_4\beta_1$ integrin. These results are summarized in Table 2.2 below.

Table 2.2: Results of fluorescence blocking assay.

Conc. $ArBF_3$-LLP2A (nM)	**Conc. FITC-LLP2A (nM)**	**Fluorescence observed**
100	1	No
100	400	No

a) 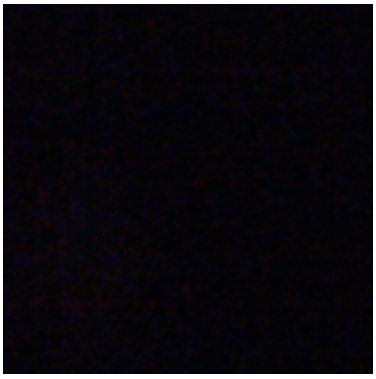 b) 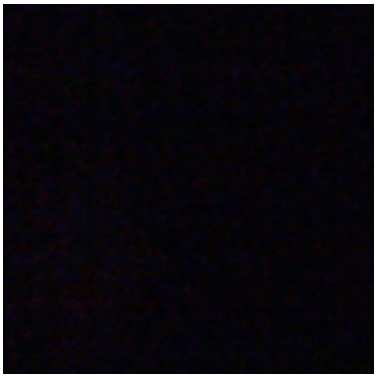

Figure 2.11: MOLT-4 cells exhibiting no fluorescence after being treated with 100 nM $ArBF_3$-LLP2A and subsequently (a) 1 nM FITC-LLP2A and (b) 400 nM FITC-LLP2A.

2.6 ^{18}F-Radiolabeling of $ArB(OR)_2$-LLP2A

2.6.1 One-step Radiolabeling

The $ArB(OR)_2$-LLP2A was then labeled under radioactive or "hot" conditions at the TRIUMF facility by Dr. Ying Li of the Perrin group. Near identical conditions to those listed for the fast fluorination (section 2.4.3) were used, except now using a $^{18/19}F$ solution. The reaction was allowed to proceed for 1 hour before being quenched with an NH_4OH solution and analyzed by RP-HPLC. The detector in this case measures radioactivity, allowing us to determine if more than one radiolabeled product is present. The radioactivity detector was able to identify only one radioactive product other than free $^{18}F^-$, shown below in the RP-HPLC trace.

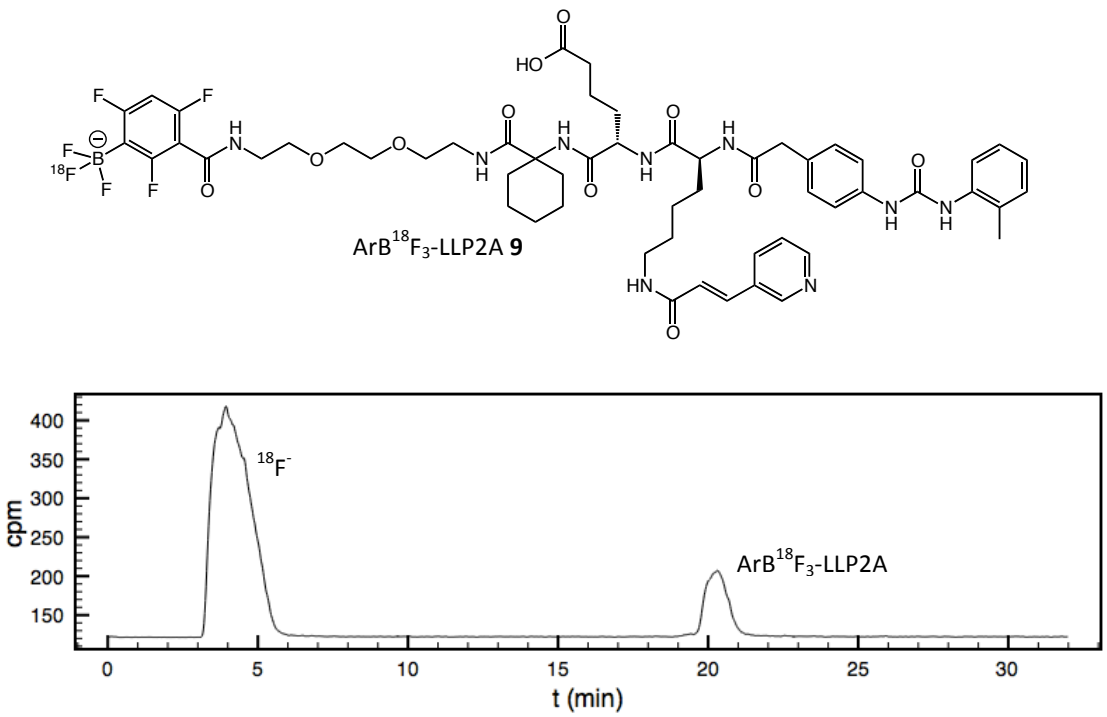

Figure 2.12: Radiolabeled product $ArB^{18}F_3$-LLP2A **9** (top) and RP-HPLC trace (bottom) of radiolabeling showing $ArB^{18}F_3$-LLP2A **9** (20 min) and free $^{18}F^-$ (4 min).

The reaction was done using $^{18/19}F$ with a specific activity of 1.96 mCi/µmol at the beginning of synthesis (BOS). At the end of synthesis (EOS), after 60 minutes, the specific activity was measured to be 1.31 mCi/µmol. 100 nmol of $ArB(OR)_2$-LLP2A was used for this reaction, with each molecule capturing three fluorides atoms, therefore tripling the specific activity of the imaging compound, yielding a radiotracer with a specific activity of 3.93 mCi/µmol.

2.6.2 Two-step Radiolabeling via Click Chemistry

The two-step click labeling of N_3-LLP2A was also investigated by Dr. Li. During the course of this project, ongoing study concerning the fluorination of boronates was performed by the Perrin group. New protecting groups for boron were considered in hopes of identifying a more acid labile protecting group that would afford higher fluorination yields. One of the more promising protecting groups was diamino naphthalene (R'). An alkynyl-modified $ArB(OR')_2$ that uses diamino naphthalene instead of 1,1,2,2-tetraphenyl pinacol (R) as a protecting group was used during the click labeling of N_3-LLP2A. The alkynyl-$ArB(OR')_2$ was first labeled under similar conditions to those used in the one-step fluorination described above in section **2.6.1**. The specific activity at the BOS was 3.68 mCi/µmol.

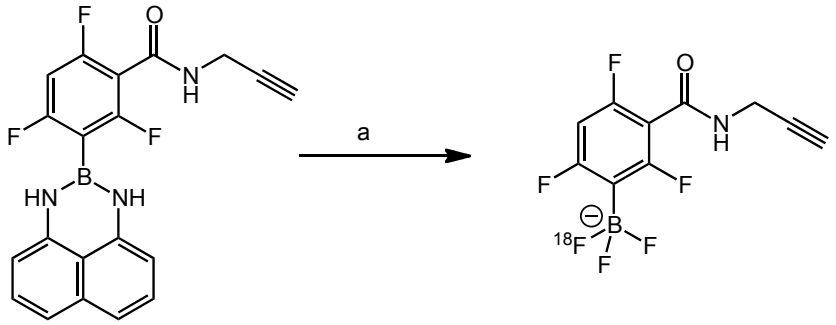

Scheme 2.17: Synthesis of alkynyl-$ArB^{18}F_3$. Reagents and conditions: a) alkynyl-$ArB(OR')_2$, $^{18/19}F_{(aq)}$, HCl, and THF reacted for 22 minutes at RT.

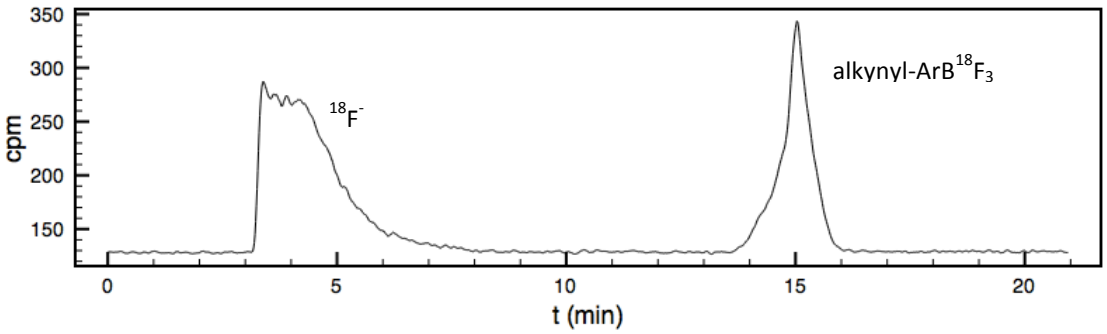

Figure 2.13: RP-HPLC of alkynyl-ArB$^{18}F_3$.

The alkynyl-ArB$^{18}F_3$ was then conjugated to N_3-LLP2A via click chemistry in a solution containing $CuSO_4$ and sodium ascorbate. The specific activity at the EOS was 2.04 mCi/µmol. When taking into account the 100 nmol of N_3-LLP2A used in this reaction, the specific activity of the labeled compound is calculated to be 6.12 mCi/µmol. The RP-HPLC analysis of the labeling reaction and the click conjugation are shown below.

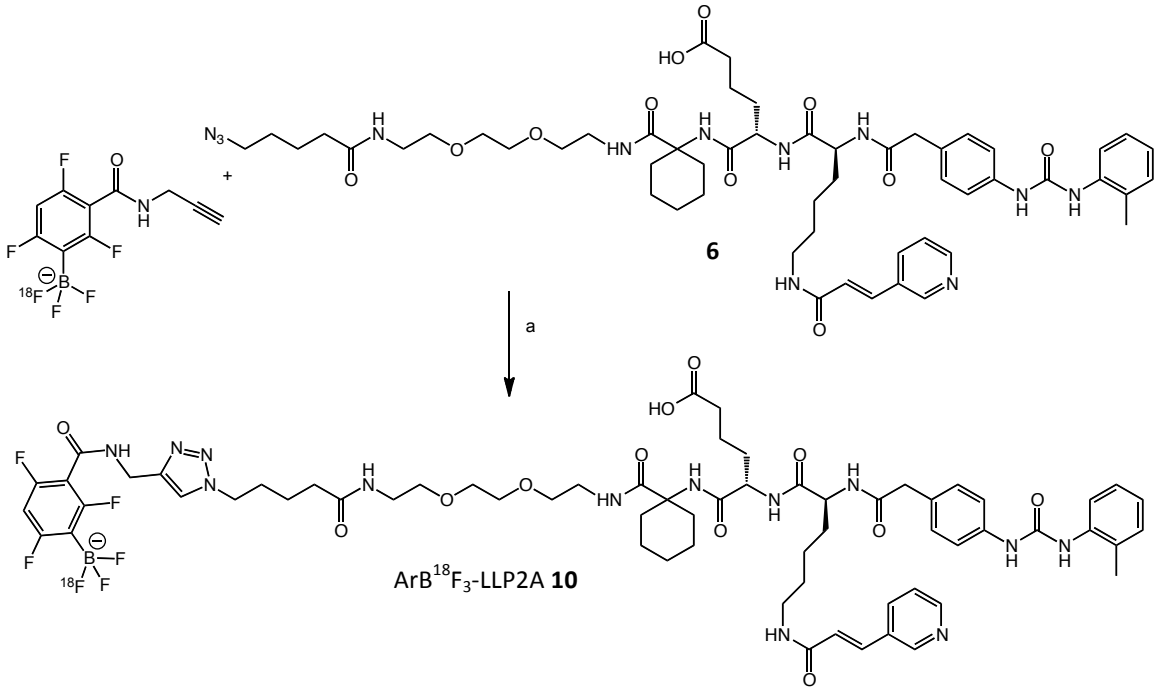

Scheme 2.18: Synthesis of the final product of the two-step radiolabeling of LLP2A. Reagents and conditions: a) alkynyl-ArB$^{18}F_3$, N_3-LLP2A, NaAsc, $CuSO_4$, $EtOH_{(aq)}$ reacted for 36 minutes at RT.

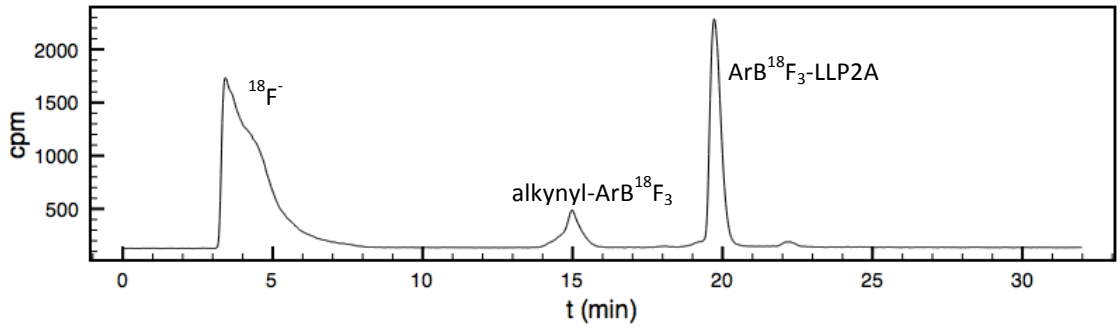

Figure 2.14: RP-HPLC of the final radiolabeled ArB$^{18}F_3$-LLP2A **10** (19 min) and alkynyl-ArB$^{18}F_3$ (15 min).

Chapter 3

Conclusions and Future Directions

3.1 Conclusions

Novel methods for imaging cancer are needed in the face of an increasingly prevalent disease that touches all corners of the globe. The replacement of ^{18}FDG with tumor-specific imaging agents such as peptides for routine PET imaging will improve both the diagnosing and prognosis of cancer patients.[9]

Perrin and colleagues have developed an innovative method of ^{18}F-labeling through aryltrifluoroborate formation under conditions that are compatible with biomolecules.[29] Aryltrifluoroborates, having been earlier found to be stable under physiological conditions,[32] open the door to previously unattainable specific activities through the capture of three ^{18}F atoms per biomolecule, effectively tripling the specific activity of the source fluoride.[31]

The $\alpha_4\beta_1$ integrin-targeting compound LLP2A[38] was synthesized on solid phase and coupled to $ArB(OR)_2$, which was then fluorinated under cold conditions to produce $ArBF_3$-LLP2A. This compound, along with the fluorescent FITC-LLP2A, was tested *in vitro* against $\alpha_4\beta_1$ expressing cells and found to be biologically active. An N_3-LLP2A was also prepared to allow for two-step labeling via click chemistry. $ArB(OR)_2$-LLP2A and N_3-LLP2A were radiolabeled by one-step and two-step methods, respectively, to produce $ArB^{18}F_3$-LLP2A. These compounds are now ready to proceed to *in vivo* imaging.

3.2 Future Directions

With the successful synthesis of $ArB^{18}F_3$-LLP2A, the immediate next step is the *in vivo* imaging of a $\alpha_4\beta_1$-expressing tumor. Discussion on collaborative imaging projects with research groups around the continent is underway. Continuing investigation into LLP2A and the aryltrifluoroborate labeling technology allows us to be optimistic that compounds based on these structures may soon find their way into clinical research trials.

The development of new boronic acid protecting groups such as diaminonapthalene grants new possibilities for one-step radiolabeling of a $ArB(OR)_2$-LLP2A. The increased acid-lability of novel protecting group may provide high yield fluorinations under milder conditions.

The azido-modified LLP2A presents several other interesting applications for this bioligand. Facile conjugation under mild conditions afforded by click chemistry have potential for use not only in imaging, but also therapeutics. The high-affinity targeting of LLP2A make it a good candidate for conjugation with a high-toxicity drug. One could envision a LLP2A ligand functionalized with both imaging and therapeutic moieties, allowing simultaneous visualization and treatment of a tumor.

Chapter 4

Experimental

4.1 Materials

All chemicals and solvents were purchased from Sigma-Aldrich, Alfa Aesar, Nova Biochem or Chem-Impex International and used without further purification, unless otherwise noted. Thin layer chromatography, both analytical and preparative, was performed on either aluminum or glass backed plates coated with Silica Gel 60 F_{254} which had been purchased from EMD Chemicals. Silica Gel 60 for chromatography was purchased from Silicycle. Spin columns for SPPS were purchased from Thermo Scientific. NMR experiments were performed in deuterated solvent purchased from Cambridge Isotope Laboratories. Distillation over sodium metal under nitrogen atmosphere was used to produce anhydrous THF. All other solvents were used as received from the vendor. Cell lines were purchased from ATCC. Cell growth medium was purchased from Invitrogen.

4.2 Techniques

4.2.1 NMR Spectroscopy

All NMR experiments were performed on a Bruker AV-300 (300 MHz) spectrometer. All NMR samples were prepared in glass vials before being transferred to an NMR tube. The solubility of each sample was tested in non-deuterated solvent prior

to sample preparation in deuterated solvent. NMR tubes from Norell were used for all experiments. All NMR spectra are referenced to the residual solvent peak in accordance with the values listed by Gottlieb *et al.*[49] Peaks for all spectra are reported as chemical shifts, δ (ppm), and multiplicity (s = singlet, d = doublet, t = triplet, m = multiplet). All data was processed using iNMR or Mnova programs.

4.2.2 Mass Spectrometry

Low resolution mass spectra were acquired using a Waters ZQ spectrometer. High resolution mass spectra were acquired by staff at the UBC Mass Spectrometry lab using a Waters/Micromass LCT time-of-flight spectrometer. All samples were prepared in either methanol or a mixture of acetonitrile and water.

4.2.3 Chromatography

TLC results are reported as R_f, describing the ratio of the distance moved by the analyte to the distance moved by solvent front. Detection of R_f was performed using a handheld UV lamp operating at both 254 and 365 nm wavelengths. In the absence of UV absorbance, or for further analyte identification, ninhydrin stain was also used. Column chromatography was conducted using Silica Gel 60 packed between two layers of sea washed sand that was purchased from Fischer Scientific.

RP-HPLC analyses are reported in minutes as retention time, t_R. An Agilent 1100 HPLC furnished with an automatic injection unit and photodiode array detector was

used to perform RP-HPLC. Both analytical and preparative style reverse phase columns were employed for purification: (1) a Phenomenex Jupiter C_{18} (250 x 4.60 mm) and (2) an Agilent Eclipse XDB-C_{18} (250 x 9.4 mm). All RP-HPLC was performed with the columns maintained at 50 °C. Three different programs, each run at 1 mL/min, were used for RP-HPLC analysis: Program 1, Program 2, and Program 3. Program 1 consists of two solvents: A) Water + 0.1 % TFA and B) ACN + 0.05 % TFA. Program 1 was carried out as follows with the mobile phase composition given as a percentage of solvent B: 30 % B over 5 min; 30 % to 90 % B over 15 min; 90 % to 100 % B over 5 min; 100 % B over 3 min, 100 % to 30 % B over 2 min; 30 % B over 2 min. Program 2 consisted of two solvents: C) Water and D) MeOH. Program 2 was carried out as follows with the mobile phase composition given as a percentage of solvent D: 15 % to 35 % D over 5 min; 35 % to 90 % D over 15 min; 90 % to 100 % D over 5 min; 100 % D over 3 min; 100 % to 50 % D over 2 min; 50 % D over 2 min. Program 3 consisted of two solvents: E) 0.04 M HCO_2NH_4 and F) ACN. Program 3 was carried out as follows with the mobile phase composition given as a percentage of solvent F: 0 to 5 % F over 5 min; 5 % to 20 % F over 5 min; 20 % to 50 % F over 10 min; 50 % to 100 % F over 5 min; 100 % to 95 % F over 3 min; 95 % to 5 % F over 2 min; 5 % F over 2 min.

4.2.4 UV-Visible Absorption

A Beckman Coulter DU800 spectrophotometer, equipped with both tungsten and deuterium lamps, was used to record all UV-Visible absorbance spectra. Samples were prepared in glass vials prior to transfer to quartz cells for testing. Transfer was

accomplished using polyethylene disposable transfer pipets purchased from Fischer Scientific. Quartz cells of 1 cm path length were purchased from Fisher Scientific.

4.2.5 Cell Proliferation

Human MOLT-4 Leukemia cells were incubated at 37 °C in 5% CO_2 atmosphere in RPMI-1640 medium containing 10% fetal bovine serum. Cells were grown in Falcon brand T-25 flasks.

4.2.6 Fluorescence Microscopy

Fluorescence microscopy was performed on an Olympus IX70 microscope.

4.3 Solid Phase Peptide Synthesis

4.3.1 Resin Techniques

4.3.1.1 Resin Loading Determination

Resin loading of amino acids was determined by DBF quantification resulting from Fmoc cleavage. Briefly, a small portion of **resin 1** was placed in a glass vial and dried overnight under vacuum. This was done in order to remove all residual solvent that could be incorrectly attributed to resin mass. The dried resin was weighed and then swollen in 1.980 mL DMF with slow stirring. After 20 minutes, 20 µL of DBU was added. This reaction was allowed to proceed for approximately 20 minutes with slow stirring. The reaction was then diluted to 10 mL with ACN. One mL of this solution was

then diluted to 13 mL with ACN. A blank solution was prepared in parallel to the procedure described above, although no resin was used. The absorbance of the solution was measured at a single wavelength, 304 nm. The molar extinction coefficient of DBF is ε = 7624 $M^{-1}cm^{-1}$. The loading of the resin was then calculated to yield an amount in mmol/g.

4.3.1.2 Resin Cleavage

All products were cleaved from the solid phase resin, for mass spectrometry analysis or product collection, using HFIP. Briefly, to the resin to be cleaved was added a 30 % solution of HFIP in DCM. The reaction was allowed to proceed for 30 minutes. The solution was separated from the resin by gravity filtration and the resin was washed with DCM. The volume of the filtrate was decreased using a rotary evaporator to yield the product.

4.3.2 Fmoc-Ach (resin 1)

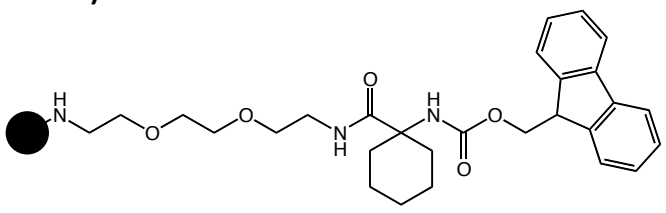

O-bis-(aminoethyl)ethylene glycol trityl resin (0.642 g) was swollen in 5 mL of DCM for 2 hours in a 10 mL RBF. The resin was transferred to a 10 mL plastic spin column and the solvent filtered off. To a glass vial was added Fmoc-Ach-OH (0.899 g,

2.46 mmol), HBTU (0.958 g, 2.52 mmol), DIPEA (0.90 mL, 5.17 mmol), and 4 mL DMF. These compounds were allowed to dissolve and this solution was added to the spin column containing the resin. The resin was gently shaken for 1 hour, after which the solution was filtered off. The resin was washed with DMF (3 x 5 mL) and DCM (3 x 5 mL) and suction dried using an aspirator for 20 minutes to afford **resin 1**. A sample of this resin was removed and the product cleaved off and dissolved in methanol for mass spectrometry analysis. The loading of **resin 1** was determined by the technique described in section 4.3.1.1 to be 0.47 mmol/g.

LRMS (ESI) *m/z*: calculated for $C_{28}H_{37}N_3O_5$ $[M+H^+]$: 496.27, found: 496.5.

4.3.3 Fmoc-Aad(*t*Bu)-Ach (resin 2)

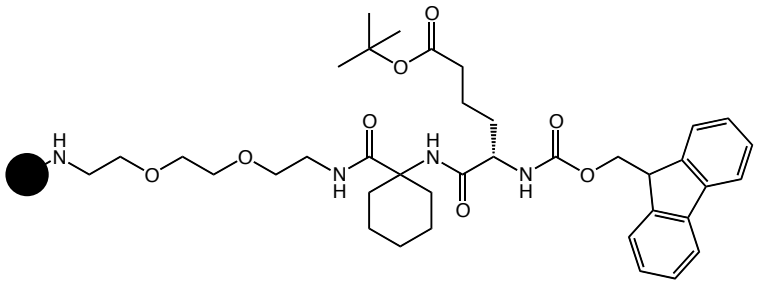

Resin 1 (0.521 g) was shaken with 7 mL of a solution of 20% piperidine in DMF for 10 minutes. The solution was removed from the resin by filtration and this procedure was repeated twice more. The resin was then washed thoroughly with DMF to afford the Fmoc-deprotected NH_2-Ach **resin 1**. To deprotected **resin 1** was added a solution of Fmoc-Aad(*t*Bu)-OH (0.530 g, 1.20 mmol), HBTU (0.468 g, 1.23 mmol), DIPEA (0.43 mL, 2.46 mmol), and 4 mL DMF. The mixture was gently shaken for 1 hour and the

solution was removed by filtration. The resin was washed with DMF (3 x 5 mL) and DCM (3 x 5 mL) and suction dried on an aspirator for 20 minutes to afford **resin 2**. A sample of this resin was removed and the product cleaved off and dissolved in methanol for mass spectrometry analysis.

LRMS (ESI) *m/z*: calculated for $C_{38}H_{54}N_4O_8$ [M+H$^+$]: 695.86, found: 695.7.

4.3.4 Fmoc-Lys(Dde)-Aad(*t*Bu)-Ach (resin 3)

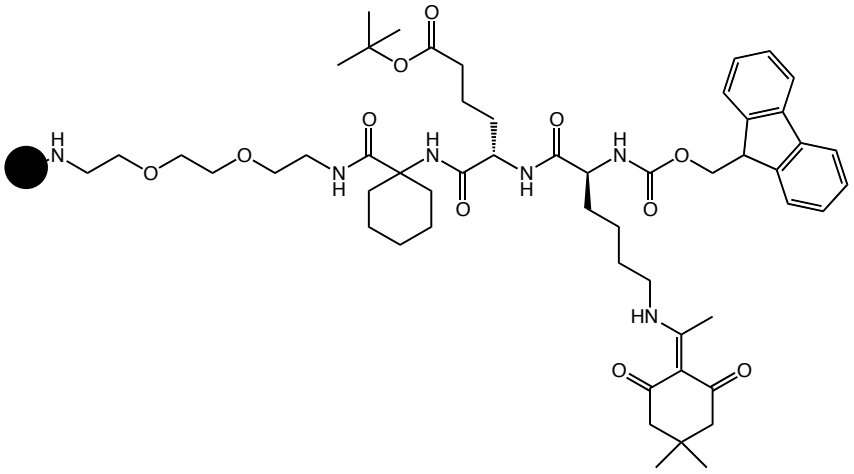

Resin 2 (0.521 g) was shaken with 7 mL of a solution of 20 % piperidine in DMF for 10 minutes. The solution was removed from the resin by filtration and this procedure was repeated twice more. The resin was then washed thoroughly with DMF to afford the Fmoc-deprotected NH_2-Aad(*t*Bu)-Ach **resin 2**. To deprotected **resin 2** was added a solution of Fmoc-Lys(Dde)-OH (0.642 g, 1.20 mmol), HBTU (0.477 g, 1.26 mmol), DIPEA (0.45 mL, 2.57 mmol), and 4 mL DMF. The mixture was gently shaken for 1 hour and the solution was then removed from the resin by filtration. The resin was washed

with DMF (3 x 5 mL) and DCM (3 x 5 mL) and suction dried on an aspirator for 20 minutes to afford **resin 3**. A sample of this resin was removed and the product cleaved off and dissolved in methanol for mass spectrometry analysis.

LRMS (ESI) *m/z*: calculated for $C_{54}H_{78}N_6O_{11}$ $[M+H^+]$: 988.23, found: 988.0.

4.3.5 2-(4-(3-*o*-tolylureido)phenyl)acetyl-Lys(Dde)-Aad(*t*Bu)-Ach (resin 4)

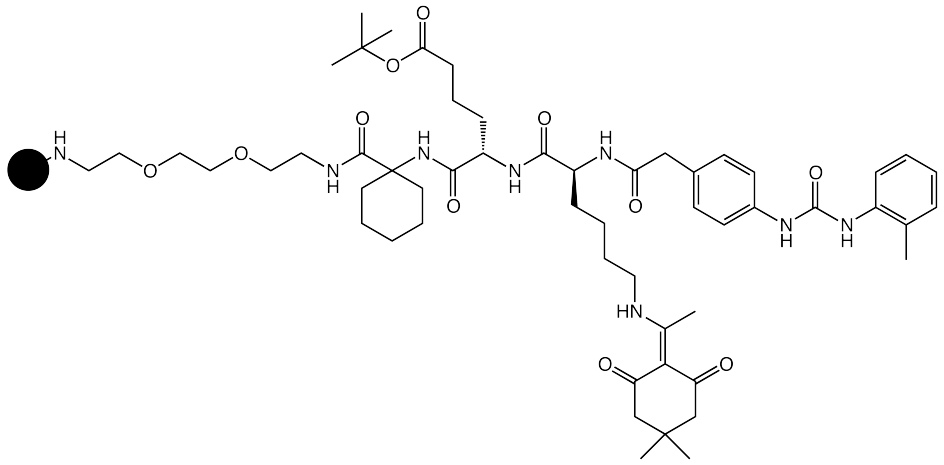

Resin 3 (0.521 g) was shaken with 7 mL of a solution of 20% piperidine in DMF for 10 minutes. The solution was removed from the resin by filtration and this procedure was repeated twice more. The resin was then washed thoroughly with DMF to afford the Fmoc-deprotected NH_2-Lys(Dde)-Aad(*t*Bu)-Ach **resin 3**. To deprotected **resin 3** was added a solution of 2-(4-(3-*o*-tolylureido)phenyl)acetic acid **1** (0.362g, 1.27mmol), HBTU (0.492 g, 1.30 mmol), DIPEA (0.45 mL, 2.57 mmol), and 4 mL DMF. The resin was gently shaken for 1 hour and the solution was then removed by filtration and the resin washed with DMF and DCM. The reaction was repeated using 0.178 g **1**,

0.251 g HBTU, and 0.25 mL DIPEA to ensure full coupling. The resin was washed with DMF (3 x 5 mL) and DCM (3 x 5 mL) and suction dried on an aspirator for 20 minutes to afford **resin 4**. A sample of this resin was removed and the product cleaved and dissolved in methanol to allow mass spectrometry analysis.

LRMS (ESI) *m/z*: calculated for $C_{55}H_{82}N_8O_{11}$ $[M+H^+]$: 1032.29, found: 1032.2.

4.3.6 [2-(4-(3-*o*-tolylureido)phenyl)acetyl]-Lys(3-(3-pyridyl) acrylyl)-Aad(*t*Bu)-Ach (resin 5)

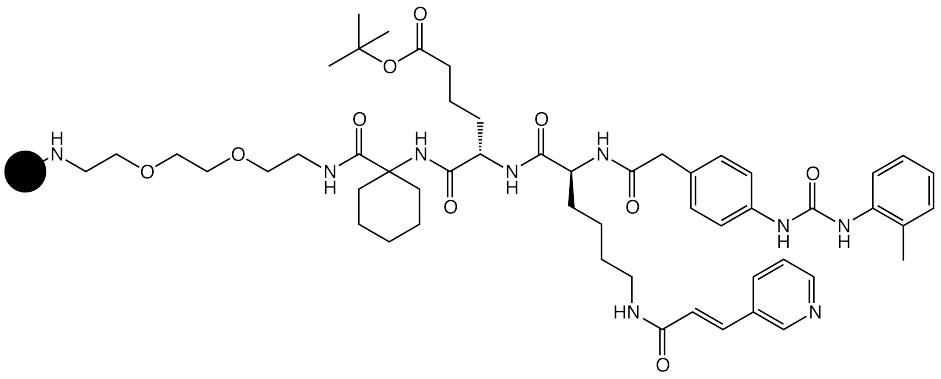

Resin 4 (0.521 g) was shaken with 5 mL of a solution of 2% hydrazine in DMF for 4 minutes. The solution was removed from the resin by filtration and this procedure was repeated twice more. The resin was then washed thoroughly with DMF to afford the Dde-deprotected [2-(4-(3-*o*-tolylureido)phenyl)acetyl]-Lys-Aad(*t*Bu)-Ach **resin 4**. To deprotected **resin 4** was added a solution of 3-(3-pyridyl)acrylic acid (0.189g, 1.27mmol), HBTU (0.489 g, 1.29 mmol), DIPEA (0.45 mL, 2.57 mmol), and 4 mL DMF. The resin was gently shaken for 1 hour and the solution was then removed by filtration. The resin was washed with DMF (3 x 5 mL) and DCM (3 x 5 mL) and suction dried on an

aspirator for 20 minutes to afford **resin 5**. A sample of this resin was removed, the product cleaved and dissolved in methanol to allow mass spectrometry analysis.

LRMS (ESI) *m/z*: calculated for $C_{53}H_{75}N_9O_{10}$ [M+H$^+$]: 999.2, found: 999.0.

4.3.7 [2-(4-(3-*o*-tolylureido)phenyl)acetyl]-Lys(3-(3-pyridyl) acrylyl)-Aad(*t*Bu)-Ach (LLP2A(*t*Bu), 2)

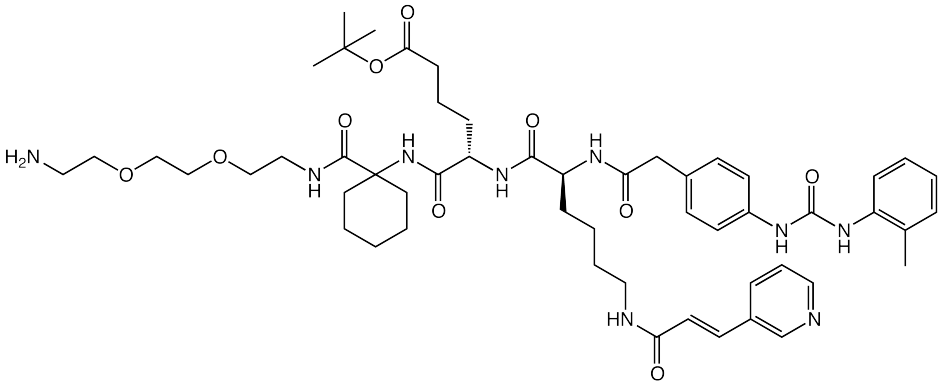

Resin 5 (0.521 g) was placed in a 25 mL RBF. 9 mL of a 30% HFIP in DCM was added to the resin and the mixture was stirred for 30 minutes. The resin was filtered off and the filtrate volume was reduced using a rotary evaporator. To the resulting yellow solution was added diethyl ether, precipitating a white solid. The solid was filtered off and dried *in vacuo*. The crude product was purified using preparative TLC (1:9 NH_4OH:EtOH) to afford product LLP2A(*t*Bu) **2** (0.020 g, 7 % yield overall), a white solid. The analytical HPLC was performed using Program 1.

HRMS (ESI) *m/z*: calculated for $C_{53}H_{75}N_9O_{10}$ [M+H$^+$]: 999.5708, found: 999.5715.

R_f = 0.61 (1:9 NH_4OH:EtOH)

t_R = 12.16 min (Program 1)

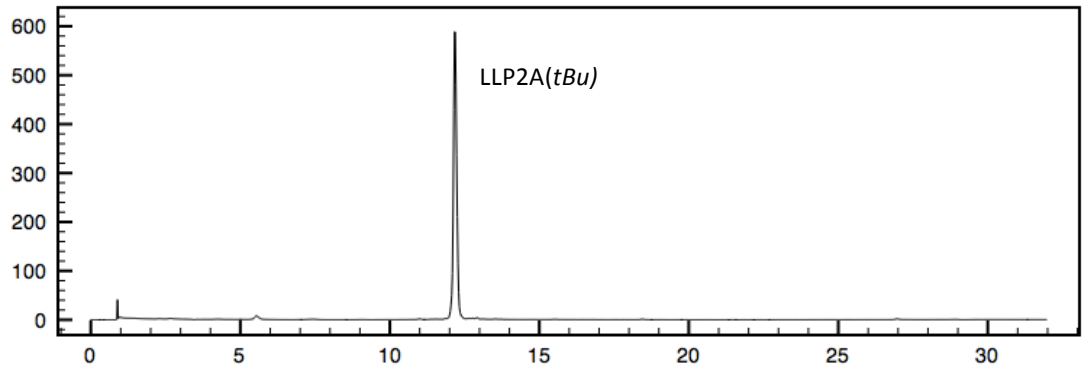

Figure 4.1: RP-HPLC trace of LLP2A(*t*Bu). Reproduced from page 44.

4.4 Synthesis in Solution

4.4.1 2-(4-(3-*o*-tolylureido)phenyl)acetic acid[38] (1)

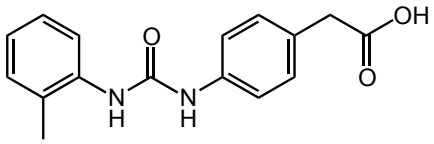

To a solution of 4-aminophenyl acetic acid (1.514 g, 10.0 mmol) and 50 mL DMF in a 250 mL RBF was added dropwise *o*-tosyl isocyanate (1.370 g, 10.3 mmol). This mixture was stirred for 2.5 hours at RT and the volume of the solvent reduced to 15 mL using a rotary evaporator. The solution was poured onto ethyl acetate (100 ml) with stirring which resulted in the formation of a light brown precipitate. This was collected by filtration and washed with ethyl acetate (2 x 25 mL) and ACN (3 x 25 mL). The solid was dried under vacuum to afford 2.085 g of tan coloured solid (73 %).

LRMS (ESI) *m/z*: calculated for $C_{16}H_{16}N_2O_3$ [M+Na^+]: 307.31, found: 307.3.

^{1}H NMR (300 MHz, DMSO d_6) δ (ppm): 2.25 (s, 3H), 3.50 (s, 2H), 6.94 (t, 1H, *J*=7.5Hz), 7.14-7.20 (m, 4H), 7.40 (d, 2H, *J*=8.5Hz), 7.84 (d, 1H, *J*=7.9Hz), 7.90 (s, 1H), 8.99 (s, 1H).

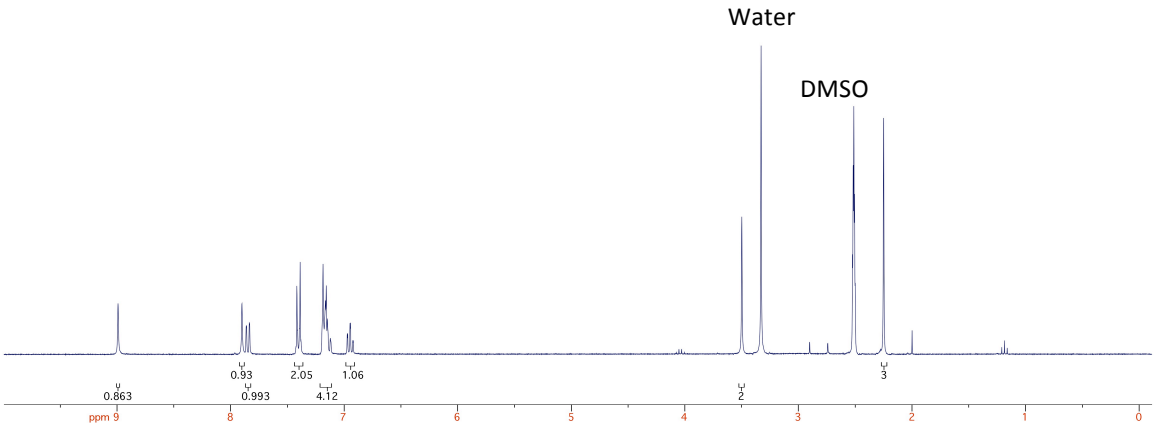

Figure 4.2: ^{1}H NMR of **1.**

4.4.2 2,4,6-Trifluoro-3-(4,4,5,5-tetraphenyl-1,3,2-dioxaborolan-2-yl)benzoic acid ($ArB(OR)_2$, 3)

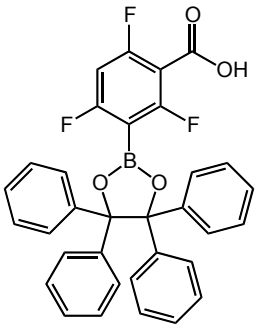

To a flame dried 100 mL RBF was added 2,4,6-trifluorobenzoic acid (0.50 g, 2.9 mmol) and 40 mL of dry THF which had been distilled over sodium metal. The solution was then cooled to -78 °C with an acetone/$CO_{2(s)}$ bath under $N_{2(g)}$ flow and stirred for 30 minutes. Following this, 4 mL of a 1.6 M solution of *n*-BuLi in hexanes (6.4 mmol, 2.2

eq.) was added drop wise over 1 hour. The solution turned orange and was left to stir for 15 minutes after addition of the *n*-BuLi. Next, trimethylborate (0.80 mL, 7 mmol) was added via a syringe and the solution was stirred for 2 hours. The reaction was then quenched with 4 mL of a 4.0 M solution of HCl in dioxane. A benzopinacol solution (1.6 g, 4.3 mmol in 10 mL THF) was then added to the reaction. The acetone/$CO_{2(s)}$ was then removed and the solution was stirred for 2 hours as it warmed to RT. 50 mL of toluene was added to the reaction and it was then concentrated. This process was repeated twice more. The resulting solid was loaded onto a 2 cm silica column, where the product was eluted using 10 % EtOAc in Hexanes. The elution was monitored by TLC and the appropriate fractions were collected to yield 0.122 g (8 %) of white solid.

LRMS (ESI) *m/z*: calculated for $C_{33}H_{22}BF_3O_4$ [M+Na^+]: 573.33, found: 573.3.

^{1}H NMR (300 MHz, $CDCl_3$) δ (ppm): 6.86 (t, 1H), 7.11 (m, 12H), 7.22 (m, 8H).

^{19}F NMR (300 MHz, $CDCl_3$) δ (ppm): -93.26 (1F), -96.10 (1F), -103.50 (1F).

R_f = 0.35 (1:9 MeOH:DCM)

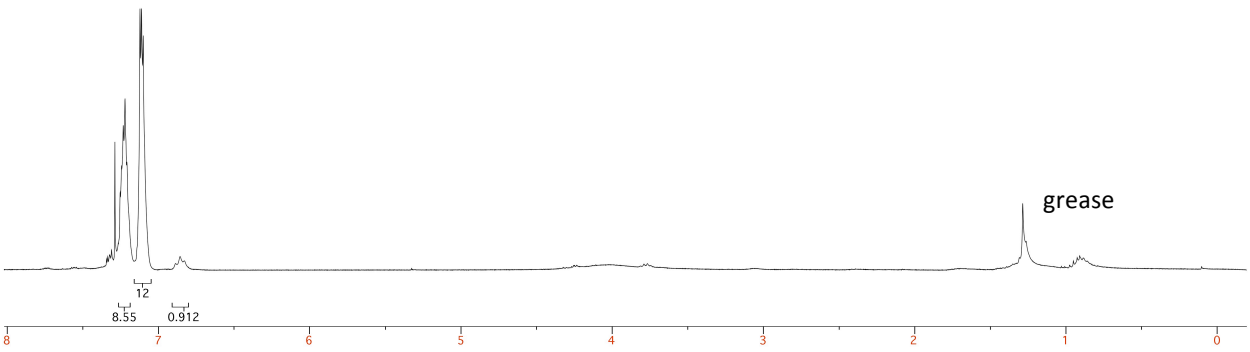

Figure 4.3: ^{1}H NMR of **3**.

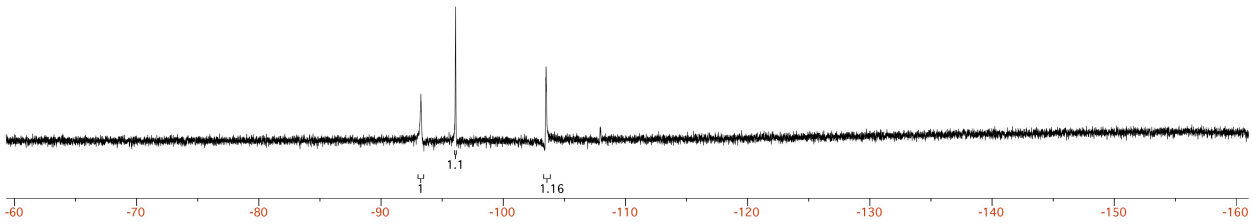

Figure 4.4: ^{19}F NMR of **3**.

4.4.3 ArB(OR)$_2$-LLP2A (4)

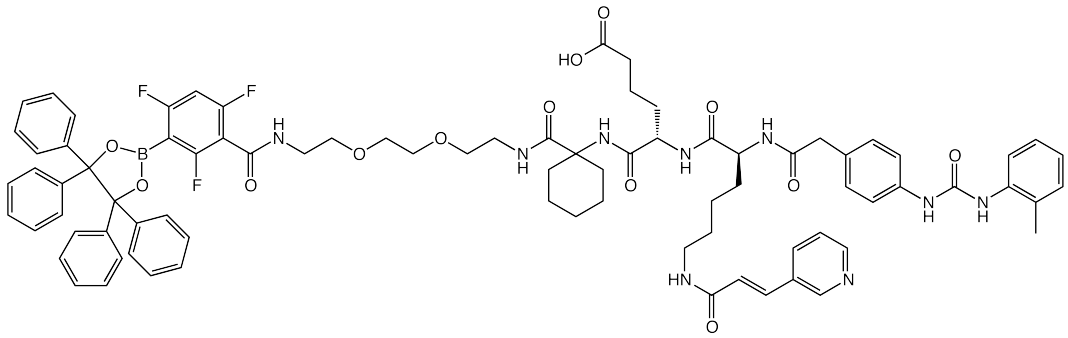

To a 5 mL RBF was added 0.75 mL DMF, LLP2A(*t*Bu) (12.5 mg, 12.5 µmol), ArB(OR)$_2$ (8.26 mg, 15.0 µmol), EDC•HCl (3.1 mg, 16.1 µmol), HOBt•H_2O (2.5 mg, 16.3 µmol) and pyridine (5.47 µL, 67.3 µmol). This solution was allowed to react over night. The solvent was then removed under vacuum and the resulting oil was dissolved in 1 mL THF. The addition of diethyl ether caused a white precipitate to form. The solution was centrifuged, the solvent was decanted and the resulting solid was dried under vacuum. To this solid was added one mL of a 50 % solution of TFA in DCM and the solution was stirred for one hour after which the solvent was removed. The resulting oil was resuspended in 0.5 mL THF and diethyl ether was added to precipitate a white solid.

The solvent was decanted and the solid dried under vacuum to afford 9.5 mg of crude product. The crude was dissolved in 0.5 mL DCM and loaded on to a 1 cm silica column and eluted with 7 % MeOH in DCM. The appropriate fractions were pooled together and the volume was reduced. The resulting oil was dissolved in 200 µL THF and precipitated with diethyl ether. This solution was centrifuged, the solvent decanted and the left over white solid was dried under vacuum to afford 6.0 mg (32.6 %) of ArB(OR)$_2$-LLP2A.

HRMS (ESI) *m/z*: calculated for $C_{82}H_{87}BF_3N_9O_{13}$ [M+H$^+$]: 1474.6572, found: 1474.6547.

R_f = 0.43 (1:9 MeOH:DCM)

t_R = 18.90 min (Program 1)

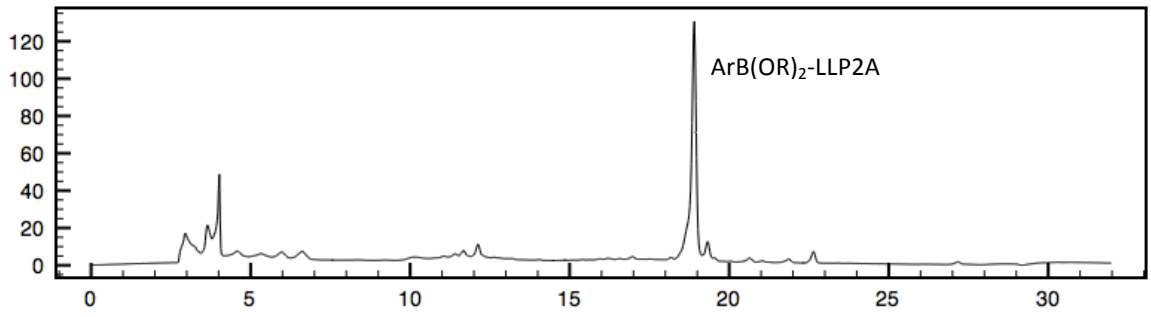

Figure 4.5: RP-HPLC trace of ArB(OR)$_2$-LLP2A.

4.4.4 5-azido pentanoic acid[46] (5)

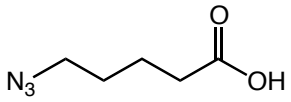

To a 10 mL RBF was added 5-bromo ethyl pentanoate (2.00 g, 9.53 mmol), 5 mL DMSO and NaN_3 (2.480 g, 38.5 mmol). This mixture was stirred for 24 hours at 100 °C. Upon cooling, the solution turned into a brown solid, which was then dissolved in 100 mL water. This solution was extracted with diethyl ether (4 x 50 mL). The organic layers were pooled together. The volume was reduced to 30 mL and the solution diluted to 60 mL with 1N NaOH. This mixture was stirred at RT overnight. The solution was then washed with ether and acidified to pH 1 with concentrated HCl. The product was extracted with ether (3 x 20 mL), dried with Na_2SO_4, and the solvent was removed under vacuum, yielding 0.933 g (68 %) of a yellow liquid.

^{1}H NMR (300 MHz, $CDCl_3$) δ (ppm): 1.6-1.8 (m, 4H), 2.41 (t, 2H), 3.31 (t, 2H).

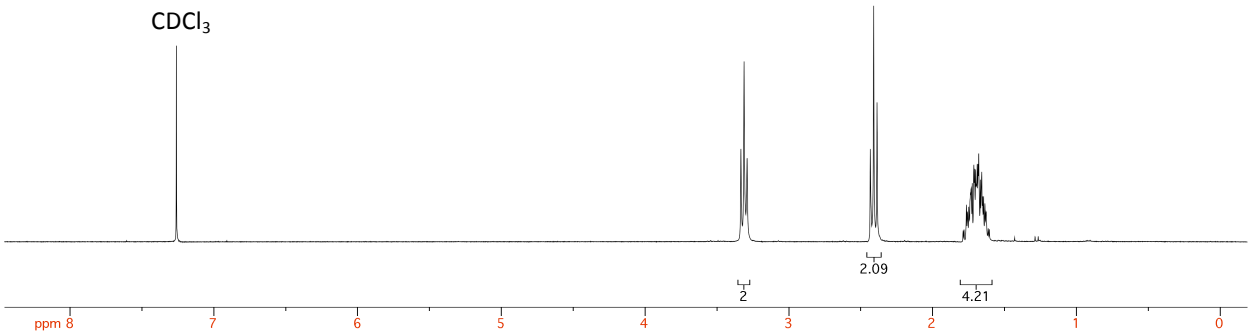

Figure 4.6: ^{1}H NMR of **5**.

4.4.5 N_3-LLP2A (6)

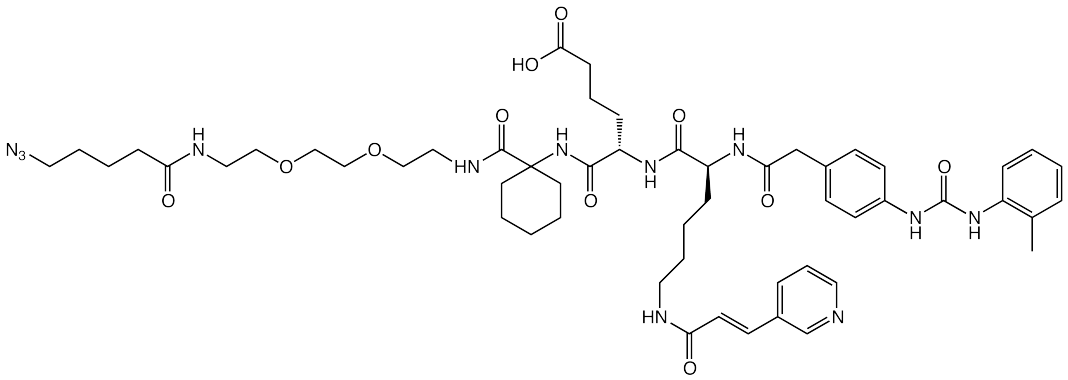

To a 5 ml RBF was added LLP2A(*t*Bu) (1.9 mg, 1.9 µmol), HBTU (4.0 mg, 10.5 µmol), 5-azido pentanoic acid (1.1 mg, 7.6 µmol), and DIPEA (1.9 mg, 15 µmol) and 2 mL of DMF. This mixture was stirred for 1 hour and the solvent was then reduced using a rotary evaporator. Addition of cold diethyl ether caused a white solid to precipitate. The vial was centrifuged and the solid pellet was collected and dried under vacuum. This product was added to a 5 mL RBF and was dissolved in 2 mL of a 50% TFA in DCM solution. The solution was stirred for 1 hour, after which the solvent was removed *in vacuo.* Diethyl ether was added to precipitate a white solid, which was separated by filtration to yield a white solid. The solid was dissolved in methanol and purified by RP-HPLC (Program 1) to afford 1.6 mg (89 %) of N_3-LLP2A.

LRMS (ESI) *m/z*: calculated for $C_{54}H_{74}N_{12}O_{11}$ $[M+H^+]$: 1068.24, found: 1068.0.

R_f = 0.76 (5:95 NH_4OH:EtOH)

t_R = 11.42 min (Program 1)

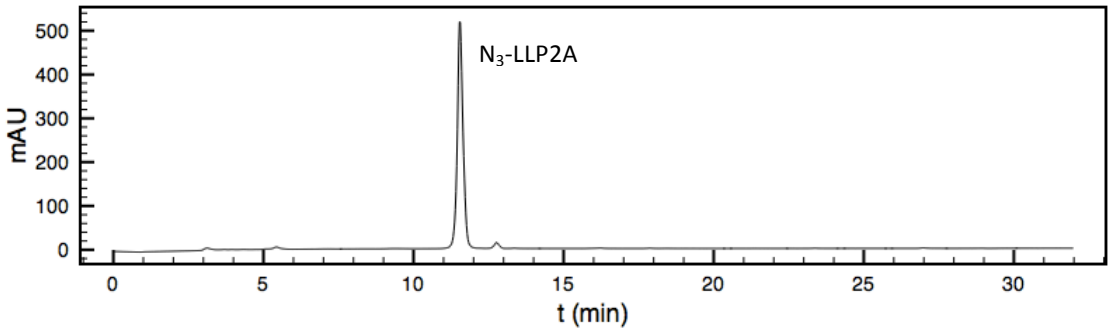

Figure 4.7: RP-HPLC trace of N_3-LLP2A.

4.4.6 $ArBF_3$-LLP2A (7)

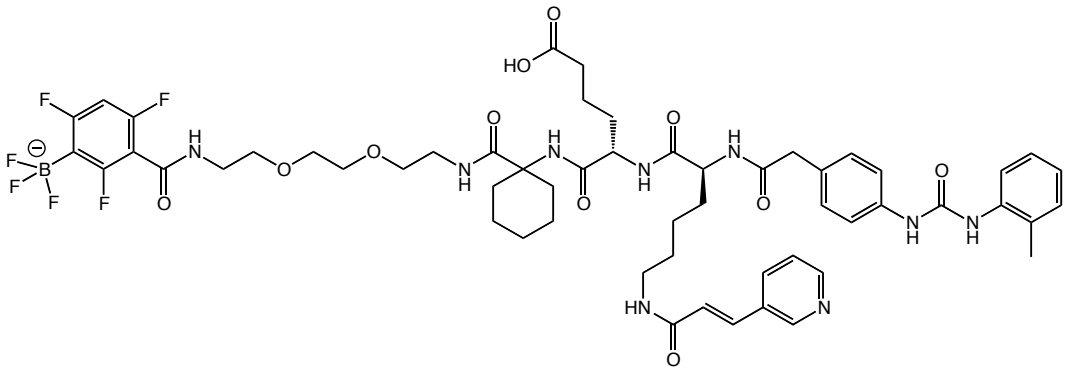

"Slow" Method

To a 1 mL eppendorf vial was added $ArB(OR)_2$-LLP2A (3.3 mg, 2.24 µmol), 200 µL THF and 15 µL (30 eq) of a 4.5 M $KHF_{2(aq)}$ solution. The vial was vortexed and the reaction was allowed to proceed overnight. The next day, a solid KHF_2 crystal was removed and the product was precipitated upon addition of diethyl ether. The solvent was decanted and the product redissolved in THF and precipitated with diethyl ether

again. The solid was collected and dried under vacuum to give 1.6 mg (57.6 %) of white solid. The HPLC was performed using Program 2.

LRMS (ESI) *m/z*: calculated for $C_{56}H_{67}BF_6N_9O_{11}$ [M-H-F]: 1146.98, found: 1147.0.

^{19}F NMR (300 MHz, $CDCl_3$) δ (ppm): -99.12 (1F), -104.16 (1F), -117.91 (1F), -132.24 (3F)

R_f = 0.25 (1:9 MeOH:DCM)

t_R = 9.18 min (Program 2)

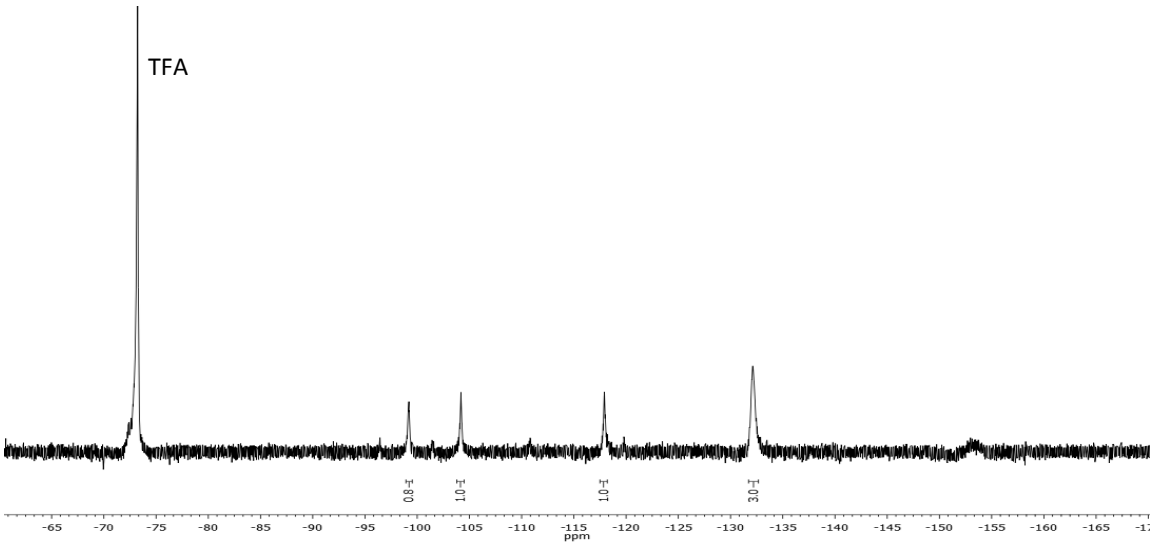

Figure 4.8: ^{19}F NMR of $ArBF_3$-LLP2A.

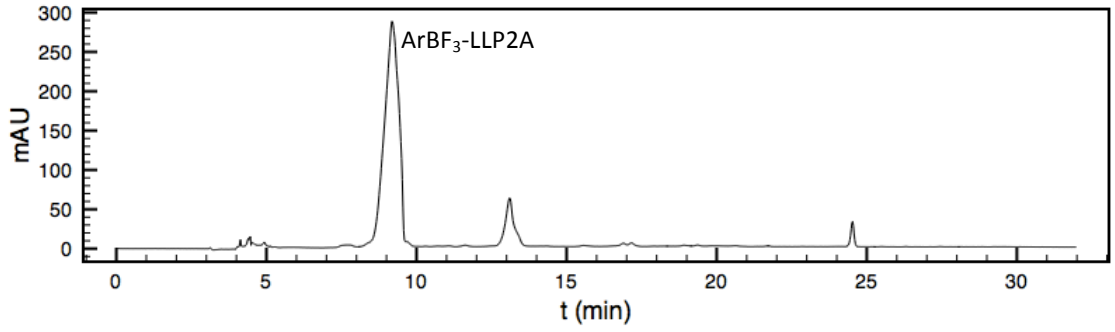

Figure 4.9: RP-HPLC trace of $ArBF_3$-LLP2A. Reproduced from page 50.

"Fast" Method

To a 0.5mL eppendorf vial containing 100 nmol of $ArB(OR)_2$-LLP2A was added 2 µL of a 0.125 M $KHF_{2(aq)}$ solution, 4 µL THF and 0.5 µL HCl. The vial was vortexed and left to react for 1 hour at RT. The reaction was quenched by addition of 100 µL of 5:15:80 NH_4OH:H_2O:EtOH. The resulting solution was transferred into a Waters MS vial and analyzed by RP-HPLC and MS. The HPLC was performed using Program 2.

LRMS (ESI) *m/z*: calculated for $C_{56}H_{67}BF_6N_9O_{11}$ [M-H-F]: 1146.98, found: 1147.1.

t_R = 9.08 min (Program 2)

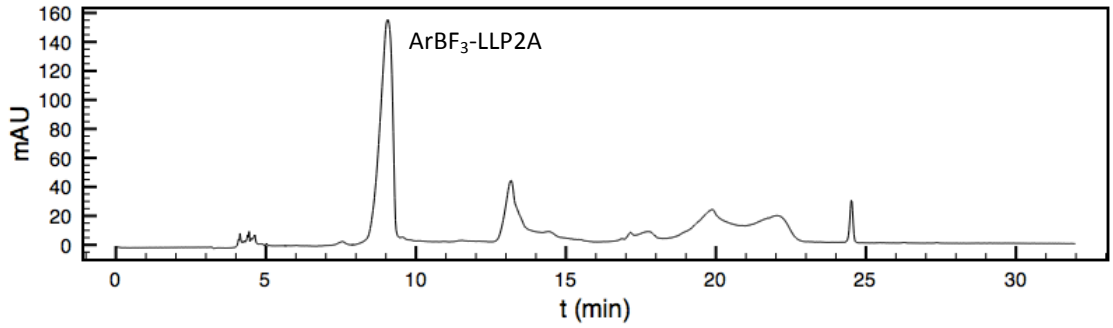

Figure 4.10: RP-HPLC of $ArBF_3$-LLP2A. Reproduced from page 52.

4.4.7 FITC-LLP2A (8)

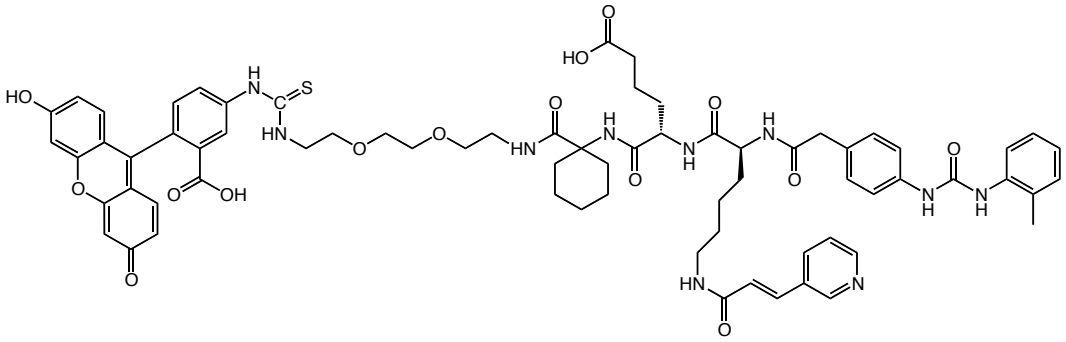

A solution of FITC (1.9 mg), 0.5 mL DMF and 0.5 mL Na_2CO_3 buffer (pH 8.4) was prepared. 0.435 mL of this solution (2.12 µmol FITC) was added to a 5 mL RBF containing 0.5 mL DMF, 0.5 mL Na_2CO_3 buffer (pH 8.4) and LLP2A(*t*Bu) (2.1 mg, 2.1 µmol). This mixture was allowed to react for 12 hours at 4 °C after which the solvent was reduced under vacuum. Addition of diethyl ether caused a yellow solid to precipitate. The vial was centrifuged and the solid pellet was collected. To this solid was added 2 mL of a 50 % solution of TFA in DCM. This mixture was allowed to react for 1 h at RT after which the solvent was removed under vacuum. The resulting solid was redissolved in 100 µL THF and precipitated with diethyl ether, then the solvent decanted and dried under vacuum to yield a yellow solid. This compound was dissolved in 3.00 mL THF and aliquoted into fractions containing 60 µL of solution. Purification of the compound by TLC took place immediately prior to use, with one aliquot providing 20 nmol of FITC-LLP2A, representing an overall reaction yield of 47 %.

LRMS (ESI) *m/z*: calculated for $C_{70}H_{78}N_{10}O_{15}S$ [M+Na^+]: 1354.49, found: 1354.3.

R_f = 0.60 (1:9 MeOH:DCM)

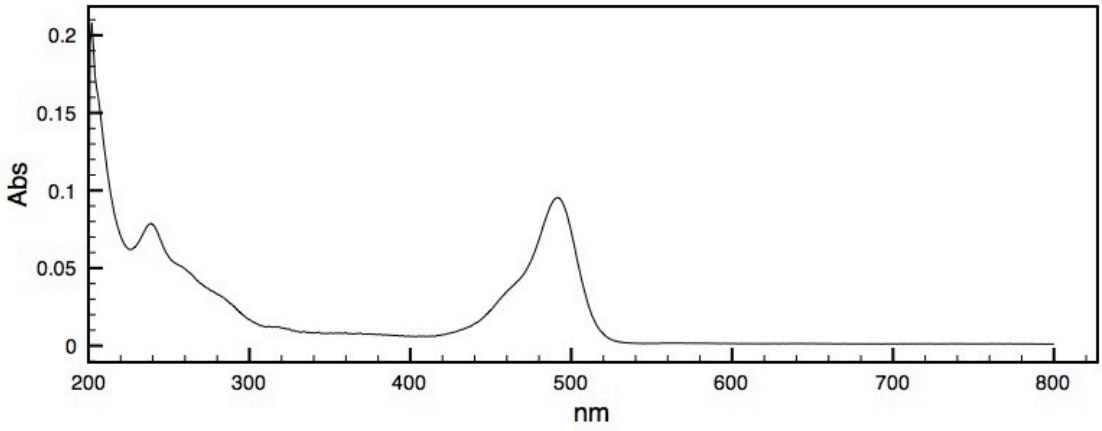

Figure 4.11: UV-visible absorption of FITC-LLP2A.

4.5 Cell Binding Assays

4.5.1 Fluorescence Assay

TBS buffer solution with 1 mM Mn^{2+} (from $MnSO_4$) and containing 400 nM FITC-LLP2A was prepared by diluting 20 nmol of FITC-LLP2A to 50 mL. 1 nM FITC-LLP2A solution was prepare by diluting 120 µL of 400 nM FITC-LLP2A to 50 mL using TBS buffer solution (1 mM Mn^{2+}). Aliquots of approximately 1 x 10^6 cells each were prepared in TBS buffer containing either 1 nM FITC-LLP2A or 400 nM FITC-LLP2A. The cells were allowed incubate for 1 hour at 37 °C, after which the mixture was transferred to a 15 mL Falcon tube. The mixture was centrifuged and the buffer was removed. The cell pellet was resuspended in fresh buffer that did not contain FITC-LLP2A, centrifuged and the buffer removed. This process was repeated once more. The cell pellet was the

resuspended in 2 mL buffer and approximately 0.3 mL was spotted on a glass slide and observed for fluorescence.

4.5.2 Blocking Assay

After several passages, aliquots of 1 x 10^6 cells each were prepared in TBS buffer (1 mM Mn^{2+}) containing 100 nM $ArBF_3$-LLP2A. After incubating for 1 hour at 37 °C, the buffer was removed and replaced with buffer containing either 1 nM FITC-LLP2A or 400 nM FITC-LLP2A. The cells were incubated for 1 hour at 37 °C, after which each mixture was transferred to a 15 mL Falcon tube. The mixtures were centrifuged and the buffer was removed. The cell pellet was resuspended in fresh buffer that did not contain FITC-LLP2A, centrifuged and the buffer removed. This process was repeated once more. The cell pellet was the resuspended in 2 mL buffer and approximately 0.3 mL was spotted on a glass slide and observed for fluorescence.

4.6 ^{18}F-Radiolabeling

The following procedures were performed by Dr. Ying Li of the Perrin group.

4.6.1 One-Step One-Pot Synthesis of $ArB^{18}F_3$-LLP2A (9)

To a PCR tube loaded with $ArB(OR)_2$-LLP2A (100 nmol), HCl (1 µL), and THF (4 µL) was added 1 µL of [$^{18/19}$F]-fluoride (507 nmol, 995 µCi at the BOS). Following incubation

for 1 hour at RT, the reaction was quenched with 100 µL of a solution of 5 % NH_4OH in 50 % aqueous EtOH. Activity was 664 µCi at the EOS. A sample of this mixture was then injected into the RP-HPLC (Program 3).

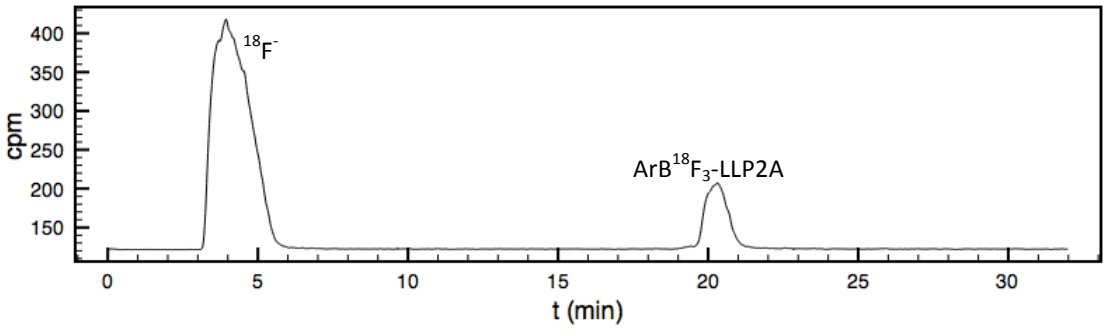

Figure 4.12: RP-HPLC radio trace of ArB$^{18}F_3$-LLP2A **9**. Reproduced from page 58.

4.6.2 One-Pot Two-Step Click Synthesis of ArB$^{18}F_3$-LLP2A (10)

To a PCR tube was added 2 µL [$^{18/19}$F]-fluoride (500 nmol, 1.84 mCi at the BOS), alkynyl-ArB(OR')$_2$ (100 nmol), HCl (0.5 µL) and 4 µL THF. The reaction was allowed to proceed at RT for 22 minutes, after which the reaction was quenched with 10 µL of a solution of 5 % NH_4OH in 50 % aqueous EtOH. A sample of this mixture (2 µL) was diluted to 100 µL using a solution of 5 % NH_4OH in 50 % aqueous EtOH for RP-HPLC analysis. The rest of the quenched reaction was then added to another PCR tube containing N_3-LLP2A (100 nmol), after which 0.6 M sodium ascorbate (4 µL) and lastly 0.2 M copper sulfate (2 µL) were also added. This reaction was allowed to proceed for 36 minutes at RT. 6 µL of the reaction was then diluted to 100 µL using a solution of 5 %

NH_4OH in 50 % aqueous EtOH. This mixture was used for RP-HPLC analysis (Program 3). Activity was 1.02 mCi at EOS.

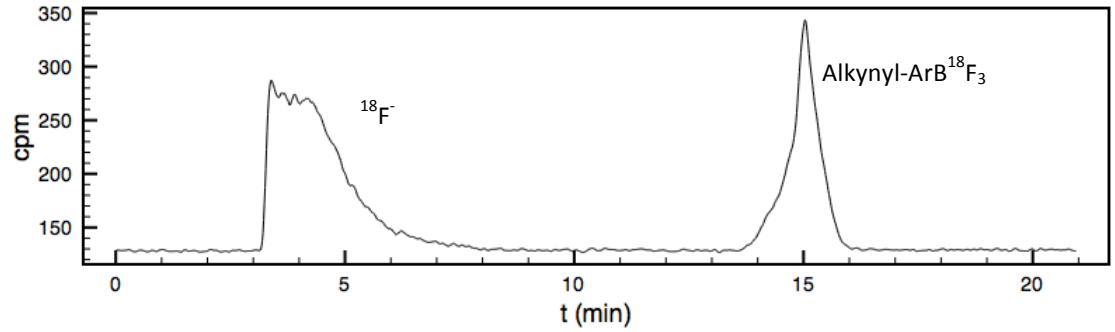

Figure 4.13: RP-HPLC of alkynyl-ArB$^{18}F_3$. Reproduced from page 60.

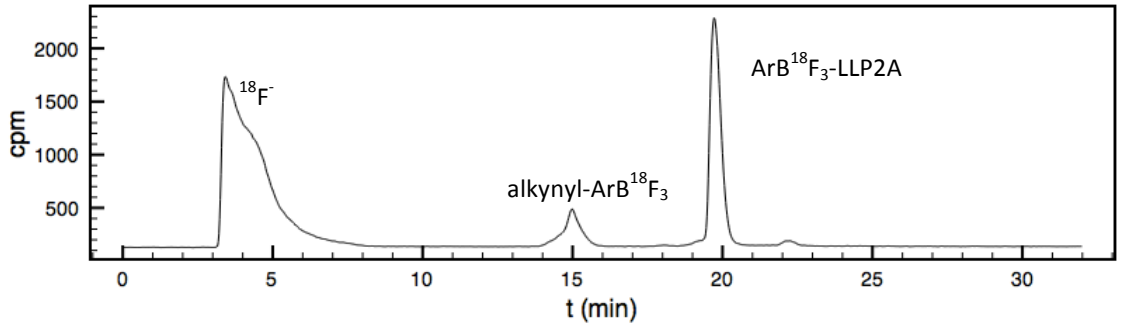

Figure 4.14: RP-HPLC of click reaction to produce ArB$^{18}F_3$-LLP2A **10**. Reproduced from page 61.

References

1. Jemal, A.; Bray, F.; Center, M. M.; Ferlay, J.; Ward, E.; Forman, D., *CA: A Cancer Journal for Clinicians* **2011,** *61* (2), 69-90.

2. *Canadian Cancer Society's Steering Committee: Canadian Cancer Statistics 2010*; Canadian Cancer Society: Toronto, 2010.

3. Achilefu, S., *Chemical Reviews* **2010,** *110* (5), 2575-2578.

4. Meikle, S. R.; Kench, P.; Kassiou, M.; Banati, R. B., *Physics in Medicine and Biology* **2005,** *50* (22), R45-R61.

5. Rahmim, A.; Zaidi, H., *Nuclear Medicine Communications* **2008,** *29* (3), 193-207.

6. Ziegler, S. I., *Nuclear Physics A* **2005,** *752* (0), 679-687.

7. Saif, M. W.; Tzannou, I.; Makrilia, N.; Syrigosa, K., *Yale Journal of Biology and Medicine* **2010,** *83*, 53-65.

8. Verboom, P.; Tinteren, H.; Hoekstra, O.; Smit, E.; Bergh, J. A. M.; Schreurs, A. M.; Stallaert, R. L. M.; Velthoven, P. M.; Comans, E. I.; Diepenhorst, F.; Mourik, J.; Postmus, P.; Boers, M.; Grijseels, E. M.; Teule, G. J.; Uyl-de Groot, C.; group, t. P. s., *European Journal of Nuclear Medicine and Molecular Imaging* **2003,** *30* (11), 1444-1449.

9. Vallabhajosula, S., *Seminars in Nuclear Medicine* **2007,** *37* (6), 400-419.

10. Cutler, P. D.; Schwarz, S. W.; Anderson, C. J.; Connett, J. M.; Welch, M. J.; Philpott, G. W.; Siegel, B. A., *Journal of Nuclear Medicine* **1995,** *36* (12), 2363-2371.

11. Le Bars, D., *Journal of Fluorine Chemistry* **2006,** *127* (11), 1488-1493.

12. Cook, G. J. R.; Maisey, M. N.; Fogelman, I., *European Journal of Nuclear Medicine and Molecular Imaging* **1999,** *26* (10), 1363-1378.

13. Sols, A.; Crane, R. K., *Journal of Biological Chemistry* **1954,** *210* (2), 581-595.

14. Rajendran, J. G.; Mankoff, D. A., *Journal of Nuclear Medicine* **2007,** *48* (6), 855-856.

15. Liu, S., *Bioconjugate Chemistry* **2009,** *20* (12), 2199-2213.

16. Wang, S.; Lee, R. J.; Mathias, C. J.; Green, M. A.; Low, P. S., *Bioconjugate Chemistry* **1996,** *7* (1), 56-62.

17. Leyton, J.; Iddon, L.; Perumal, M.; Indrevoll, B.; Glaser, M.; Robins, E.; George, A. J.; Cuthbertson, A.; Luthra, S. K.; Aboagye, E. O., *Journal of Nuclear Medicine* **2011,** *52* (9), 1441-8.

18. Wilkinson, J. A., *Chemical Reviews* **1992,** *92* (4), 505-519.

19. Becaud, J.; Mu, L.; Karramkam, M.; Schubiger, P. A.; Ametamey, S. M.; Graham, K.; Stellfeld, T.; Lehmann, L.; Borkowski, S.; Berndorff, D.; Dinkelborg, L.; Srinivasan, A.; Smits, R.; Koksch, B., *Bioconjugate Chemistry* **2009,** *20* (12), 2254-2261.

20. Roehn, U.; Becaud, J.; Mu, L.; Srinivasan, A.; Stellfeld, T.; Fitzner, A.; Graham, K.; Dinkelborg, L.; Schubiger, A. P.; Ametamey, S. M., *Journal of Fluorine Chemistry* **2009,** *130* (10), 902-912.

21. Jacobson, O.; Zhu, L.; Ma, Y.; Weiss, I. D.; Sun, X.; Niu, G.; Kiesewetter, D. O.; Chen, X., *Bioconjugate Chemistry* **2011,** *22* (3), 422-428.

22. Vaidyanathan, G.; Zalutsky, M. R., *Bioconjugate Chemistry* **1994,** *5* (4), 352-356.

23. Glaser, M.; Arstad, E., *Bioconjugate Chemistry* **2007,** *18* (3), 989-993.

24. Li, Z.-B.; Wu, Z.; Chen, K.; Chin, F. T.; Chen, X., *Bioconjugate Chemistry* **2007,** *18* (6), 1987-1994.

25. Hausner, S. H.; Marik, J.; Gagnon, M. K. J.; Sutcliffe, J. L., *Journal of Medicinal Chemistry* **2008,** *51* (19), 5901-5904.

26. Thonon, D.; Kech, C.; Paris, J.; Lemaire, C.; Luxen, A., *Bioconjugate Chemistry* **2009,** *20* (4), 817-823.

27. Kolb, H. C.; Finn, M. G.; Sharpless, K. B., *Angewandte Chemie International Edition* **2001,** *40* (11), 2004-2021.

28. Vedejs, E.; Chapman, R. W.; Fields, S. C.; Lin, S.; Schrimpf, M. R., *The Journal of Organic Chemistry* **1995,** *60* (10), 3020-3027.

29. Ting, R.; Adam, M. J.; Ruth, T. J.; Perrin, D. M., *Journal of the American Chemical Society* **2005,** *127* (38), 13094-13095.

30. Ting, R.; Lo, J.; Adam, M. J.; Ruth, T. J.; Perrin, D. M., *Journal of Fluorine Chemistry* **2008,** *129* (5), 349-358.

31. Ting, R.; Harwig, C. W.; Lo, J.; Li, Y.; Adam, M. J.; Ruth, T. J.; Perrin, D. M., *The Journal of Organic Chemistry* **2008,** *73* (12), 4662-4670.

32. Ting, R.; Harwig, C.; auf dem Keller, U.; McCormick, S.; Austin, P.; Overall, C. M.; Adam, M. J.; Ruth, T. J.; Perrin, D. M., *Journal of the American Chemical Society* **2008,** *130* (36), 12045-12055.

33. Whittaker, M.; Floyd, C. D.; Brown, P.; Gearing, A. J. H., *Chemical Reviews* **1999,** *99* (9), 2735-2776.

34. auf dem Keller, U.; Bellac, C. L.; Li, Y.; Lou, Y.; Lange, P. F.; Ting, R.; Harwig, C.; Kappelhoff, R.; Dedhar, S.; Adam, M. J.; Ruth, T. J.; Benard, F.; Perrin, D. M.; Overall, C. M., *Cancer Research* **2010,** *70* (19), 7562-7569.

35. Aina, O. H.; Sroka, T. C.; Chen, M.-L.; Lam, K. S., *Peptide Science* **2002,** *66* (3), 184-199.

36. Garmy-Susini, B.; Jin, H.; Zhu, Y.; Sung, R. J.; Hwang, R.; Varner, J., *The Journal of Clinical Investigation* **2005,** *115* (6), 1542-51.

37. Olson, D. L.; Burkly, L. C.; Leone, D. R.; Dolinski, B. M.; Lobb, R. R., *Molecular Cancer Therapeutics* **2005,** *4* (1), 91-99.

38. Peng, L.; Liu, R.; Marik, J.; Wang, X.; Takada, Y.; Lam, K. S., *Nature Chemical Biology* **2006,** *2* (7), 381-389.

39. Lam, K. S.; Salmon, S. E.; Hersh, E. M.; Hruby, V. J.; Kazmierski, W. M.; Knapp, R. J., *Nature* **1991,** *354* (6348), 82-84.

40. Liu, R.; Marik, J.; Lam, K. S., *Journal of the American Chemical Society* **2002,** *124* (26), 7678-80.

41. Park, S.; Renil, M.; Vikstrom, B.; Amro, N.; Song, L.-w.; Xu, B.-l.; Lam, K., *Letters in Peptide Science* **2001,** *8* (3), 171-178.

42. Lin, K.-c.; Ateeq, H. S.; Hsiung, S. H.; Chong, L. T.; Zimmerman, C. N.; Castro, A.; Lee, W.-c.; Hammond, C. E.; Kalkunte, S.; Chen, L.-L.; Pepinsky, R. B.; Leone, D. R.; Sprague, A. G.; Abraham, W. M.; Gill, A.; Lobb, R. R.; Adams, S. P., *Journal of Medicinal Chemistry* **1999,** *42* (5), 920-934.

43. Peng, L.; Liu, R.; Andrei, M.; Xiao, W.; Lam, K. S., *Molecular Cancer Therapeutics* **2008,** *7* (2), 432-437.

44. Carpino, L. A.; Han, G. Y., *Journal of the American Chemical Society* **1970,** *92* (19), 5748-5749.
45. Santini, R.; Griffith, M. C.; Qi, M., *Tetrahedron Letters* **1998,** *39* (49), 8951-8954.

46. Khoukhi, N.; Vaultier, M.; Carrie, R., *Tetrahedron* **1987,** *43* (8), 1811-1822.

47. Mould, A. P.; Askari, J. A.; Barton, S.; Kline, A. D.; McEwan, P. A.; Craig, S. E.; Humphries, M. J., *Journal of Biological Chemistry* **2002,** *277* (22), 19800-19805.

48. Dransfield, I.; Cabanas, C.; Craig, A.; Hogg, N., *The Journal of Cell Biology* **1992,** *116* (1), 219-226.

49. Gottlieb, H. E.; Kotlyar, V.; Nudelman, A., *The Journal of Organic Chemistry* **1997,** *62* (21), 7512-7515.